ABSTRACT

Title of Thesis: THE ROLE OF NEUROGENIN2 AND NEUROD1, AND THEIR DOWNSTREAM TARGETS, IN TRIGEMINAL GANGLION DEVELOPMENT

Parinaz Bina, Master of Science 2022

Thesis Directed By: Professor Lisa Taneyhill, Department of Animal and Avian Sciences

Abstract:

The trigeminal ganglion contains the cell bodies of sensory neurons comprising cranial nerve V and functions to relay information related to pain, touch, and temperature from the face and head to the central nervous system. Like other cranial ganglia, the trigeminal ganglion is composed of neuronal derivatives of two critical embryonic cell types, neural crest cells and placode cells. Neurogenesis within the cranial ganglia is promoted by Neurogenin2, which is expressed in trigeminal placode cells and their neuronal derivatives, and transcriptionally activates neuronal differentiation genes like *Neuronal Differentiation 1* (or *NeuroD1*). Other targets downstream of Neurogenin2 and NeuroD1 include *Drebrin1* and *Stathmin2*, cell polarity and cytoskeletal regulators that mediate changes in neuron cell shape during neurogenesis. Little is known,

however, about the role of Neurogenin2, NeuroD1, and their downstream signaling pathways during trigeminal gangliogenesis in the chick embryo. By depleting Neurogenin2 and NeuroD1 from chick trigeminal placode cells with morpholino antisense oligonucleotides, we examined how these proteins influence chick trigeminal ganglion development. Additionally, we identified the expression of Drebrin1 and Stathmin2 in trigeminal ganglion neurons. Taken together, our results highlight, for the first time, functional roles for Neurogenin2 and NeuroD1 during chick trigeminal gangliogenesis. These studies will not only improve our understanding of the molecular mechanisms underlying trigeminal ganglion development, but may also provide insight into human and animal diseases of the peripheral nervous system.

THE ROLE OF NEUROGENIN2 AND NEUROD1, AND THEIR DOWNSTREAM TARGETS, IN TRIGEMINAL GANGLION DEVELOPMENT

by

Parinaz Bina

Thesis submitted to the Faculty of the Graduate School of the
University of Maryland, College Park, in partial fulfillment
of the requirements for the degree of
Master of Science
2022

Advisory Committee:
Professor Lisa Taneyhill, Chair
Assistant Professor Andrew Broadbent
Assistant Professor Younggeon Jin

Dedication

This thesis is dedicated to my husband, Pirazh, my parents, Mojtaba and Shirin Bina, who have been a continuous source of support and encouragement throughout the challenges of graduate school and life.

Acknowledgements

First and foremost, I would like to express my sincere appreciation and gratitude to Prof. Lisa Taneyhill, my graduate adviser, for her unwavering support during my graduate studies and research. Her broad understanding of the field and extensive experience provided invaluable guidance, and I have enjoyed numerous helpful and thought-provoking conversations with her. Without her encouragement and assistance, this thesis would not have been feasible.

I would also like to thank the members of the Taneyhill lab, past and present, for creating such a conducive environment and atmosphere to study together and learn from each other. I would especially like to acknowledge Caroline Halmi for her support, generosity with her time, and helpful advice on this journey. I also want to thank Carrie Leonard, Ankita Shah, Maggie Hines, Johena Sanyal, and Seth Hannah who shaped my research in many ways.

I want to express my gratitude to my committee members Dr. Andrew Broadbent and Dr. Younggeon Jin for agreeing to serve on my thesis committee. They provided insightful feedback to improve this thesis. I am grateful to Prof. William Jeffery, Tom Porter, and Wenxia Song for their input and fruitful discussions. I was fortunate to receive valuable feedback from them.

My gratitude also extends out to Sandra Nola and Prof. Carol Keefer for their support and insight that helped me find my way in graduate school.

I would like to extend my gratitude to Prof. King-Wai Yau. In so many ways, the guidance he provided played a significant role in who I am today. The opportunities he provided me are beyond measure, and I am ever so grateful.

Finally, I would like to express my sincerest gratitude to my family and friends, who have continuously supported and encouraged me.

I hope my graduate school experience will enable me to become a better person.

Table of Contents

List of Figures

List of Abbreviations

BDNF	Brain-derived neurotrophic factor
bHLH	Basic Helix-Loop-Helix
CG	Ciliary ganglion
DBN1	Drebrin1
DMEM	Dulbecco's Modified Eagle Medium
E	Embryonic day
EB	End-binding protein
FB	Forebrain
g or gg	Geniculate ganglion
HH	Hamburger and Hamilton
HB	Hindbrain
mmV	Maxillomandibular
MB	Midbrain
MO	Morpholino
NeuroD	Neuronal Differentiation
Neurog	Neurogenin
NGF	Nerve growth factor
NHLH1	Nescient Helix-Loop-Helix 1
NT-3	Neurotrophin-3
OcN	Oculomotor nerve
OphN	Ophthalmic nerve
opV	Ophthalmic
OV	Otic vesicle
p	Petrosal ganglion
PBS	Phosphate-buffered saline
PBST	Phosphate-buffered saline with Triton
PFA	paraformaldehyde
Pl	placode
PTW	Phosphate-buffered saline with Tween
PVDF	Polyvinylidene fluoride membrane
qPCR	Quantitative polymerase chain reaction
r	Rhombomere
SDS-PAGE	Sodium dodecyl sulfate–polyacrylamide gel electrophoresis
ss	Somite stage
STMN2	Stathmin2
t or TG	trigeminal ganglion
Trk	Tropomyosin receptor kinase
TUNEL	Terminal deoxynucleotidyl transferase dUTP nick end labeling
UTR	Untranslated region

Chapter 1: Literature review

1.1 Introduction

As embryonic development progresses, various transcription factors, chemical morphogen gradients, and differential gene expression play an increasingly important role in controlling cellular morphogenesis, cell movement, and signaling. These processes lead to the formation of germ layers. Precise coordination of genetic programs allows for the development of complex tissues and organs during embryonic patterning. Understanding how these programs regulate cellular functions in space and time is still one of the major challenges in developmental biology. My thesis explores how the basic helix-loop-helix (bHLH) transcription factors, Neurogenin2 (also known as Neurog2) and NeuroD1, contribute to neurogenesis and tissue development in vertebrates, which will reveal more about how complex structures are generated during early development.

Chicken embryos serve as a suitable model for vertebrate development due to their relatively large size, easy access to the embryo due to the egg's external development, and fast growth. In addition, methods used in this system such as *in ovo* electroporation allow for easy manipulation of gene expression, providing researchers with new avenues for studying the roles of specific genes during development by using gain- and loss-of-function approaches. Consequently, the chick model has enabled researchers to discover a number of molecular pathways and regulatory networks associated with vertebrate development. Several of these mechanisms are conserved across vertebrates, making this model generalizable across species.

1.2 Neural crest cells contribute to tissues and organs during development.

In vertebrates, neurogenesis begins with the formation of the neural plate, which is a single-cell layer extending along the body axis. The two halves of the neural plate fuse together and form the neural tube. The neural tube is the structure that generates the central nervous system of vertebrates (Crane and Trainor et al., 2006).

Neural crest cells arise at the border between the nonneural ectoderm and the neural ectoderm, commonly known as the neural plate border, eventually residing within the dorsal-most region of the neural folds or neural tube. Neural crest cells are multipotent, giving rise to a variety of different cell types, including neurons and glia, craniofacial cartilage and bone, muscle cells, and gland cells (Kuriyama and Mayor, 2008). Therefore, neural crest cells play an important role in the formation of various structures and organs, including the skin, face, neck, peripheral nervous system, heart, and adrenal gland (Bronner and Simões-Costa, 2016). During development, neural crest cells undergo an epithelial-to-mesenchymal transition, a process in which stationary, epithelial cells transdifferentiate into motile mesenchymal cells (Duband et al., 1995) (Figure 1).

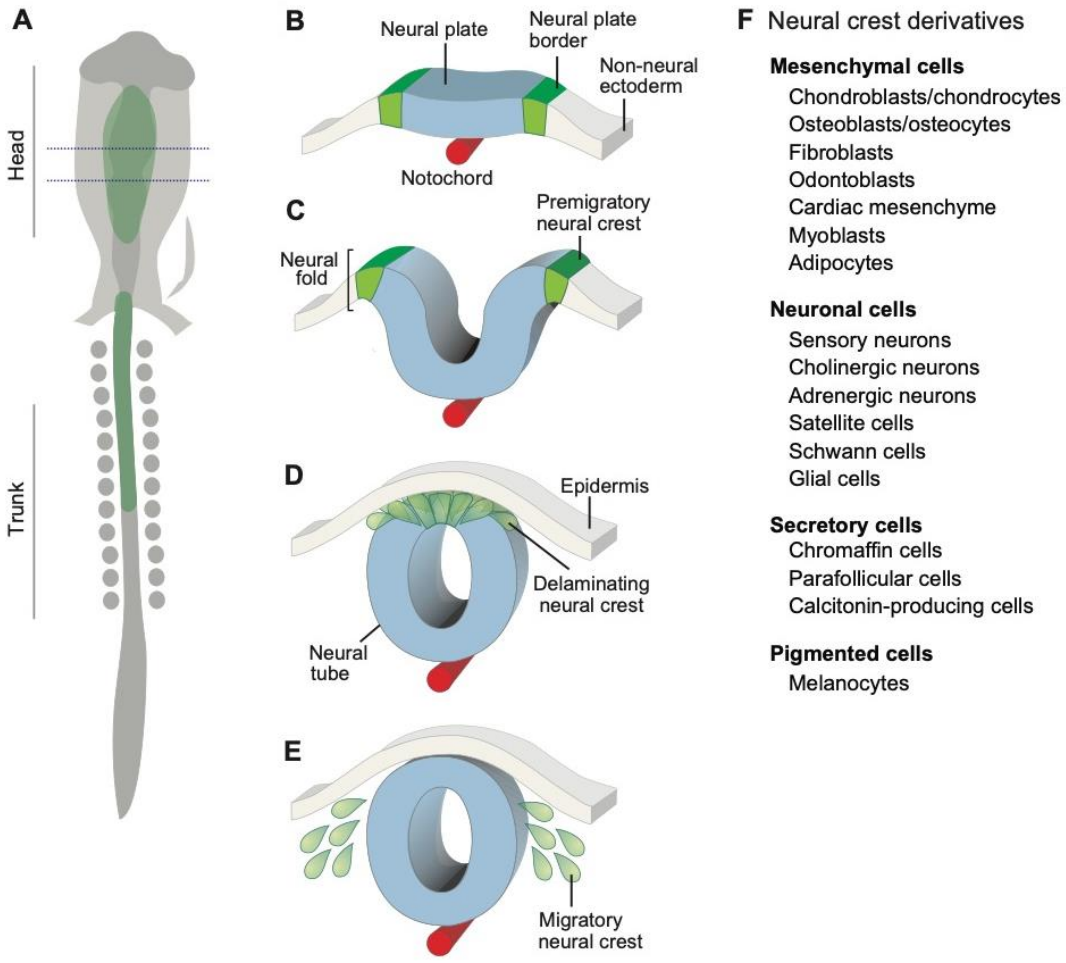

Figure 1. Neural crest cell formation and derivatives. Neural crest cells originate from the dorsal-most portion of the neural folds. Neural crest cells are initially immotile. They eventually undergo an epithelial-to-mesenchymal transition, migrate extensively, and differentiate into diverse cell types. Adapted from (Simões-Costa and Bronner, 2015).

1.3 Placode cells give rise to neurons and other structures of the sensory nervous system of the head and neck.

Cranial placodes, which exist in specific locations in the head of vertebrate embryos, are transitory, distinct regions of thickened ectoderm. Cranial placodes play an essential role in the formation of the paired sense organs such as the nose, eyes, and ears (Baker and Bronner-Fraser, 2001). During development, the epibranchial and trigeminal placodes give rise to sensory neurons of the cranial ganglia. The trigeminal placode is comprised of the ophthalmic and maxillomandibular placodes (Baker and Bronner-Fraser, 2001; Schlosser and Gerhard, 2014) (Figure 2). These sensory neurons transmit touch, pain, and temperature stimuli from the skin of the face, jaws, and teeth to the central nervous system (Baker and Bronner-Fraser, 2001). During trigeminal ganglion formation, trigeminal placode cells detach from the epithelium and migrate to the trigeminal ganglion anlage (Lassiter et al., 2014). In the chick, ophthalmic placode cells become post-mitotic as early as embryonic day (E)1 (HH8), prior to their delamination, whereas maxillomandibular placode cells become post-mitotic between E2.5 and E7 (HH16-30) (McCabe et al., 2009). After delamination, multipolar trigeminal neurons, possessing many protrusions from the cell membrane, mature and become bipolar, with only two protrusions present (Goodman et al., 1979; Shiau et al., 2011; Smith et al., 2015; Shah et al., 2017). However, the molecular mechanisms underlying these morphological changes are unknown.

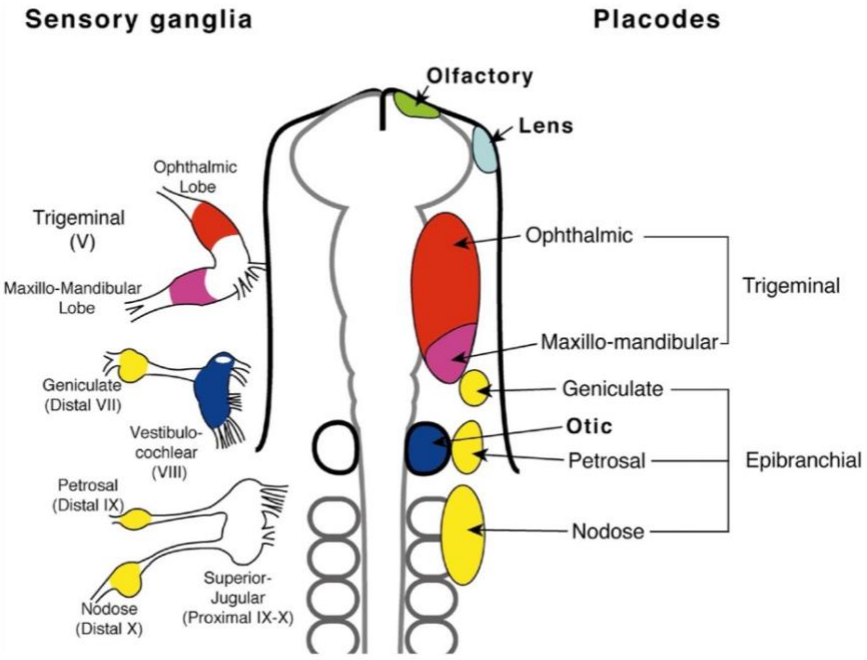

Figure 2. The neurogenic cranial placode fate map of the chick embryo. The trigeminal and epibranchial placodes (right) and their contribution to sensory neurons on the distal ganglia of cranial nerves V (trigeminal), VII, IX, and X (left). Adapted from (Baker and Bronner-Fraser, 2001).

1.4 The trigeminal ganglion contains sensory neurons derived from both neural crest cells and placode cells.

In all vertebrates, cranial nerve V is derived from the trigeminal ganglion, which houses both the cell bodies of trigeminal sensory neurons arising from neural crest cells and placode cells (Figure 3) and supporting glial cells, also of neural crest origin (Xu et al., 2008). Initial studies in birds revealed that small neurons of neural crest origin are located proximally while large neurons with a placode origin are found distally in both the ophthalmic and maxillomandibular lobes of the trigeminal ganglion (Hamburger, 1961). Experiments performed on chick embryos after neural crest cell ablation showed that the placodal neurons are scattered and form two disconnected ganglia, compared to wildtype embryos, which indicates the importance of neural crest cells as an aggregating center (Hamburger, 1961). On the other hand, placodal neurons are fundamental for formation of the neural crest-derived neurons in the trigeminal ganglion (Baker and Bronner-Fraser, 2001). In chick embryos, ophthalmic neurons appear first at E1 (HH8) followed by the appearance of the maxillomandibular placode cells starting at E2.5 (HH16) (McCabe et al., 2009). By E2.5-3 (HH16-17), placode cell-derived neurons and neural crest cells are intermixed in the condensed trigeminal ganglion, with axons aligned along the proximodistal axis (Shiau et al., 2008). Neural crest cells, however, will not differentiate into neurons until E4 (HH22-24) (Shiau et al., 2008). Placodal neurons are guided inward, and their axons innervate the hindbrain (Begbie and Graham, 2001), a process mediated by streams of neural crest cells stemming from the neural tube adjacent to the hindbrain. Freter et al. later showed that neural crest cells form corridors defining the path of the placodal neurons from the epithelium towards the hindbrain (Freter et al., 2013).

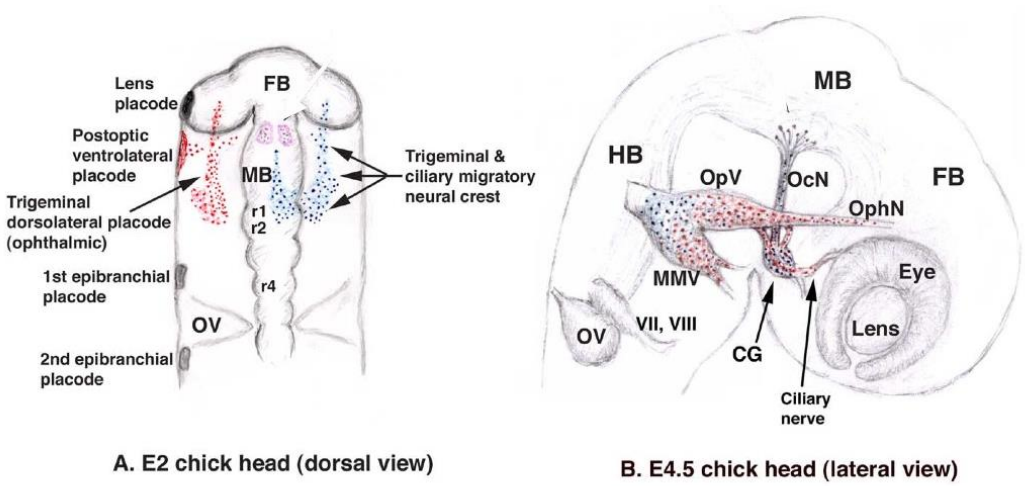

Figure 3. Schematic diagrams of the contribution of neural crest cells (blue) and placode cells (red) to chick trigeminal ganglion formation. The left diagram shows a dorsal view of a young (E2) embryo, while the right diagram shows a lateral view of an older (E4.5) embryo with two sensory branches of the trigeminal ganglion. Abbreviations: CG, ciliary ganglion; FB, Forebrain; HB, hindbrain; MB, midbrain; OcN, oculomotor nerve; OphN, ophthalmic nerve; OV, otic vesicle; r1, rhombomere 1; r2, rhombomere 2; r4, rhombomere 4. Adapted from (Lee et al., 2003).

1.5 Neurogs are neural bHLH transcription factors that are essential in neurogenesis.

Proneural genes encode bHLH proteins that are transcription factors essential in different aspects of development, specifically in cell type determination and terminal differentiation (Lee et al., 1995). These master transcription factors control neurogenesis within vertebrates (Hardwick et al., 2015). One type of bHLH proteins are the Neurogs, which are expressed in the placodal ectoderm before delamination of neuroblasts and function to regulate subsets of sensory neuron precursors (Perez et al., 1999). Neurogs also play a crucial role in neuroblast delamination and also in controlling the expression of downstream bHLH genes that support neuronal differentiation, such as *NeuroD1* (Lee et al., 1995; Ma et al., 1998). *Neurogs* may in fact function as vertebrate neuronal determination genes, particularly since they alone are adequate to transform *Xenopus* ectodermal cells into neurons, according to gain-of-function experiments (Ma et al., 1996).

Studies 20 years ago showed *Neurog2* expression only in the ophthalmic placode of chick embryos (Figure 4; Dude et al., 2009), while *Neurog1* was found in the maxillomandibular placode (Figure 5; Begbie et al., 2002). The expression of *Neurogs* differs between chick and mouse neurogenic placodes. Ma et al. (1998) showed that *Neurog1* is expressed in and required for the formation of the trigeminal and vestibuloacoustic sensory neurons in mouse, while studies from Fode et al. (1998) indicated that *Neurog2* is expressed in and essential for normal development of the epibranchial neurons in mouse. In the chick embryonic placodal ectoderm prior to delamination, Abu-Elmagd et al. (2001) noted cells expressing *Neurog1* and *NeuroD1* (Figure 6). The expression of these genes decreases as placode-derived cells mature, while *NeuroD1* expression remains in ganglion cells up to E8.

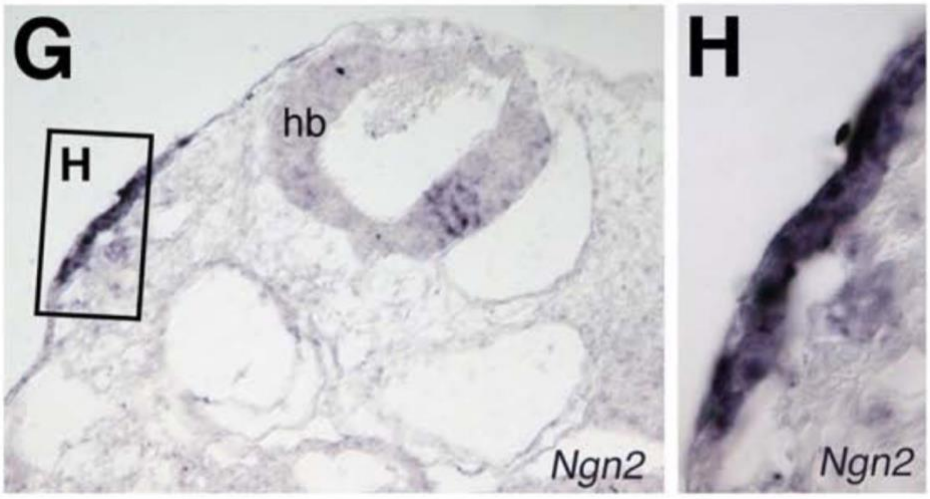

Figure 4. *Neurog2* expression in ophthalmic placode cells. Transverse section through the hindbrain of an ~E1 chick embryo (26-33 hours after laying) demonstrating *Neurog2* (formerly known as "*Ngn2*") expression (blue) in ophthalmic placode cells. Abbreviations: hb, hindbrain. Adapted from (Dude et al., 2009).

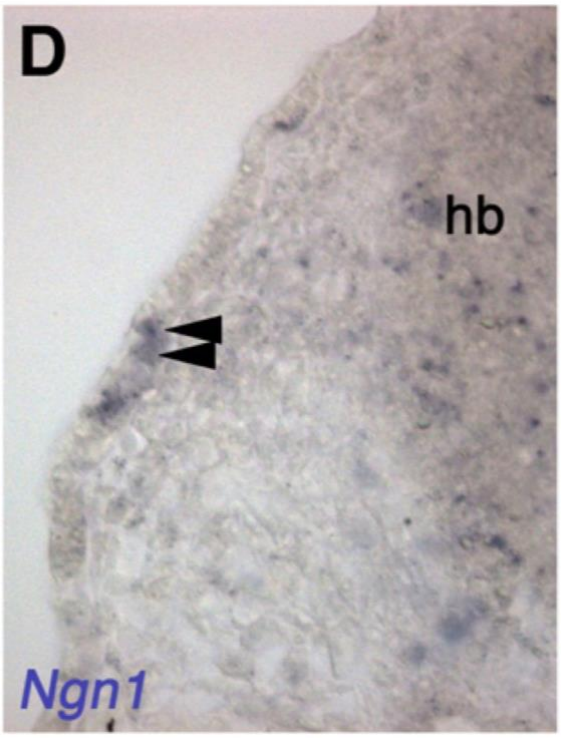

Figure 5. *Neurog1* expression in maxillomandibular placode cells. Transverse section through the hindbrain of an E2 chick embryo (45-49 hours after laying) demonstrating *Neurog1* (formerly known as "*Ngn1*") expression (blue) in maxillomandibular placode cells. Abbreviations: hb, hindbrain. Adapted from (Xu et al., 2008).

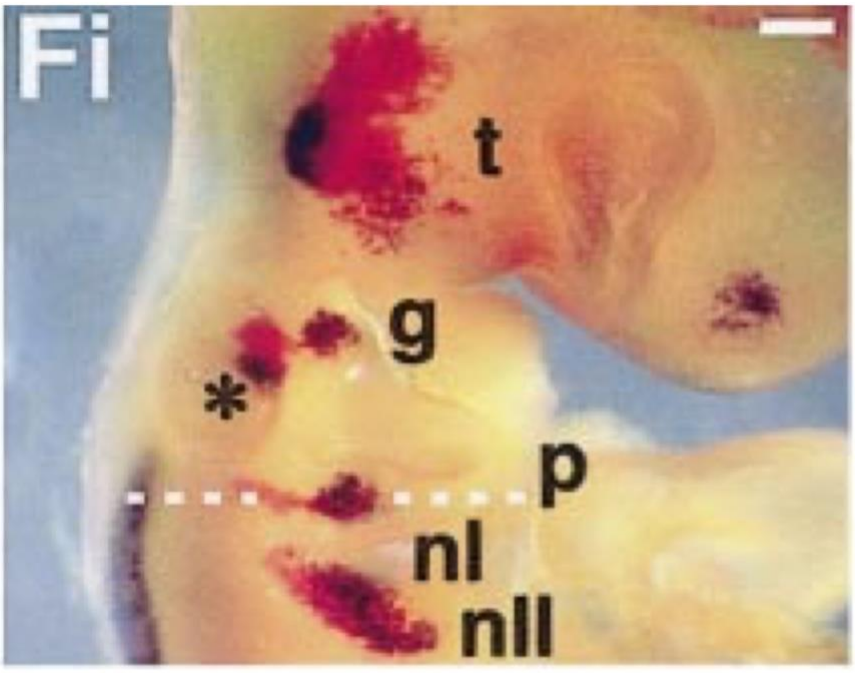

Figure 6. *Neurog1* and *NeuroD1* expression in the chick trigeminal ganglion. Double whole-mount *in situ* hybridization showing *Neurog1* (blue) and *NeuroD1* (red) expression in the chick embryo at ~E3 (65-59 hours after laying). Abbreviations: t, trigeminal ganglion; g, geniculate ganglion; p, petrosal ganglion. Adapted from (Abu-Elmagd et al., 2001).

In a study using human pluripotent stem cells, knocking down *NeuroD1* impaired the morphology of cells and increased the presence of multipolar neurons compared to control cells, but did not affect the commitment to a neuronal cell fate. Thus, the authors concluded that NeuroD1 has a significant effect on the formation of bipolar (mature) neurons (Busskamp et al., 2014). *Xenopus* embryos have also been extensively studied with regards to the expression and function of *Neurog1* and *NeuroD1* in placode cells and their derivatives. *NeuroD1* expression initially appears in scattered cells within the inner ectodermal layer of placodes and is maintained in ganglion cells that originate from these placodes (Brugmann and Moody, 2005). Interestingly, overexpression of *NeuroD1* promoted premature differentiation of neuronal precursors in *Xenopus* embryos and transformed presumptive epidermal cells into neurons (Lee et al., 1995). Fode et al. (1998) also showed that loss of Neurogs in mouse prevents delamination of placodal neurons from the epithelium due to the absence of downstream bHLH gene expression including *NeuroD1* and *NeuroD4* (Figure 7 and 8). Protein products of these bHLH genes are essential in regulating expression of other transcription factors as well as controlling the assembly and arrangement of cytoskeletal structures necessary for neuronal differentiation and migration (Seo et al., 2007). Cytoskeletal changes like these are critical for neurons to make axons and dendrites from initially immature neurites. During neurite outgrowth, rearrangements of actin filaments and microtubules occurs, as the tips of growing axons are highly dynamic (Dent et al., 2011).

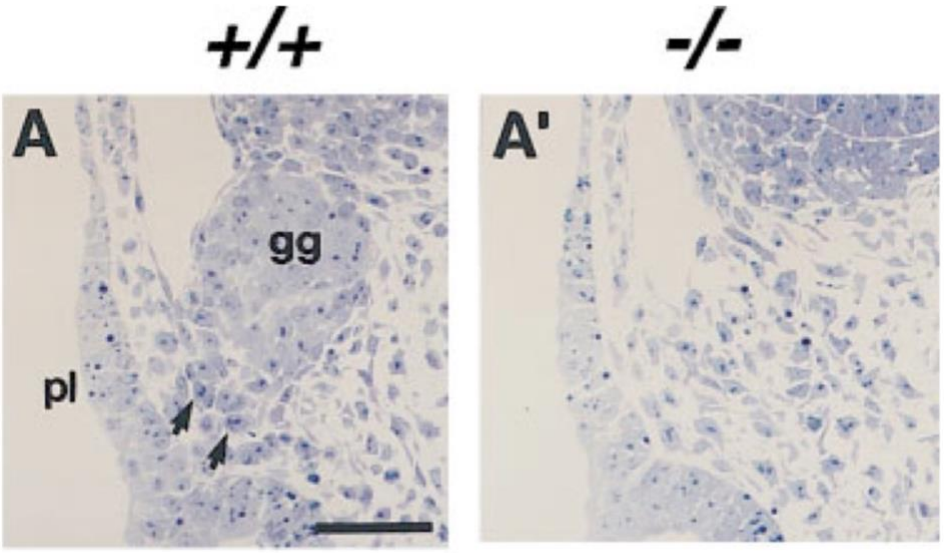

Figure 7. Blocked placodal precursor delamination in *Neurog2* mutant mice. A histological image of a section through the geniculate placode and ganglion of an embryo at E9.5. A wildtype embryo (A) showing epibranchial placodes (pl), geniculate ganglion (gg), and migrating neuronal precursors (arrows) on their way to developing into the ganglionic primordial. In *Neurog2* mutants (A'), there is no evidence of placode cell delamination, migration, or aggregation. Scale bar, 100µm. Adapted from (Fode et al.,1998)

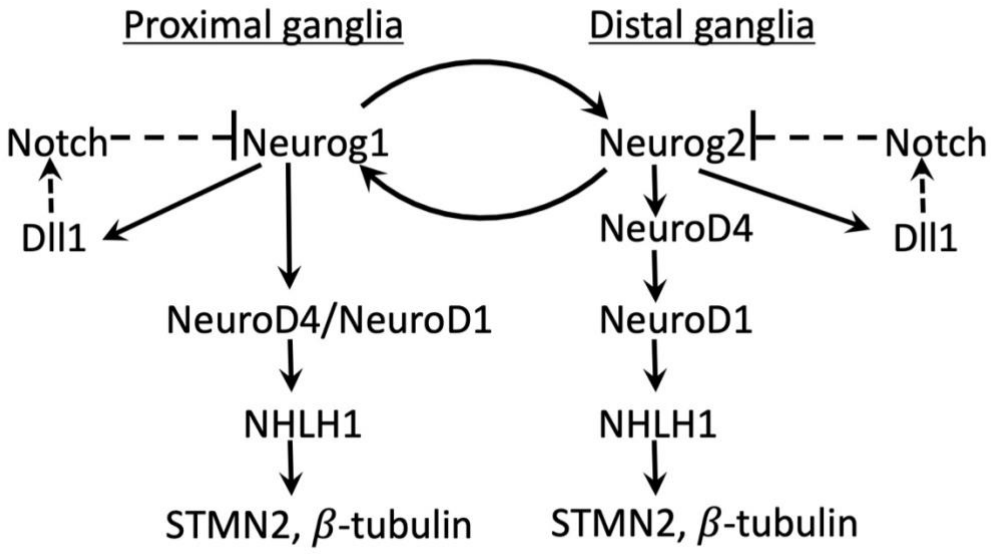

Figure 8. Summary of the regulatory interactions revealed by analysis of *Neurog* mutant mice. Activation of Neurogs triggers expression of a cascade of bHLH factors such as NeuroD4, NeuroD1, NHLH1. Abbreviation: NHLH1, Nescient Helix-Loop-Helix 1. Adapted from (Ma et al., 1998).

1.6 Downstream targets of Neurog2 and NeuroD1 control cell morphology.

Many of the downstream targets of bHLH signaling, such as Drebrin1 (DBN1) and Stathmin2 (STMN2), control cell morphology (Seo et al., 2007). Since STMN2 and DBN1 are expressed in trigeminal neurons (Chapter 5), they could be targets of NeuroD1 and/or Neurog2 signaling. Although there have been strides towards understanding the expression and activities of neural bHLH transcription factors, molecular mechanisms underlying their role(s) in neurogenesis regulation are not well understood, particularly in the trigeminal ganglion.

Microtubules are important components of the neuronal cytoskeleton, and STMN2 is critical in regulating the polymerization of microtubules (Theunissen et al., 2021). This protein is enriched in growth cones, which contain highly dynamic microtubules (Grenningloh et al., 2004). STMN2 expression is correlated with neurite outgrowth and is a potent microtubule-destabilizing protein. In the absence of STMN2 function, neurite extension and growth cone motility are reduced (Grenningloh et al., 2004). STMN2 is believed to be a downstream target of Neurog2 based on *in situ* hybridization experiments in mice (Ma et al., 1998). As demonstrated in Figure 8, expression of *NeuroD1* depends on expression of *Neurogs* in the cranial ganglia. This is also followed by the activation of other bHLH factors and ultimately by expression of structural genes specific to neurons such as *STMN2*.

In developing neurons, DBN1 is largely expressed in growth cones and is required for neuron delamination through its regulation of cytoskeletal dynamics, as it binds to both F-actin and the microtubule-binding protein EB3 (Dun et al., 2012; Geraldo et al., 2008). Based on the experiments of Seo et al. (2007) in *Xenopus*, *DBN1* is a direct target of NeuroD1. *DBN1* gain-and-loss-of-function experiments in rat cultured embryonic cortical neurons showed that

increased levels of DBN1 induced neuritogenesis, while reduced DBN1 delayed neuritogenesis (Poobalasingam et al., 2022).

In summary, like other cranial ganglia, the trigeminal ganglion consists of two distinct cell types, neural crest cells and placode cells. Prior studies in mice have shown that *Neurog2* is vital for the development of epibranchial cranial sensory ganglia, and that *Neurog2* null mutations impair the delamination of neuronal precursors from the placodes (Fode et al., 1998). *Neurog1*-deficient mice also fail to develop a trigeminal ganglion (Ma et al., 1998). Additionally, Neurogs play a key role in activating downstream bHLH factors, and that the downstream signaling pathways control the cytoskeletal regulatory proteins DBN1 and STMN2. Little is known, however, about Neurog2, NeuroD1, or the downstream signaling pathways of these proteins during the development of the trigeminal ganglion in chick embryos.

Throughout the following chapters, we describe our experiments designed to examine the role of Neurog2 and NeuroD1 in regulating chick trigeminal ganglion development and neurogenesis. The results of our studies reveal for the first time the functionality of Neurog2 and NeuroD1 during chick trigeminal gangliogenesis. These results will lead to an improved understanding of trigeminal ganglion development and shed light on diseases of the nervous system in humans and animals.

Chapter 2: Materials and Methods

2.1 Chicken embryos

Fertilized chicken eggs (Gallus gallus) were obtained from both Centurion Poultry, Inc. (Lexington, GA) as well as the University of Maryland (College Park, MD) and incubated at 37°C in humidified incubators. After approximately 38 hours of incubation, eggs were removed from the incubator and a window was made in the shell to access the embryo. Staging was conducted according to the Hamburger and Hamilton staging table (Hamburger and Hamilton, 1951). Manipulations were performed on embryos at approximately E1.5 between the 8 somite stage (ss) to 10ss (Hamburger and Hamilton (HH) stage 9^{+} through to HH10). Embryos at E2 (HH13) and older were subsequently collected for analyses.

2.2 Electroporation and morpholinos

Generally, a translation-blocking morpholino antisense oligonucleotide (MO) (Figure 9) is approximately 25 base pairs and targets the start codon of a gene of interest (Moulton and Yan, 2008). Watson-Crick base pairing allows translation-blocking MOs to bind to complementary nucleotide sequences in the 5' untranslated region and/or surrounding the start codon of the transcript of interest (Corey and Abrams, 2001). As mature ribosomes have the ability to displace bound MOs from their RNA targets, MOs interfere with translation by acting before the large ribosomal subunit attaches to the small ribosomal subunit and forms the mature ribosome. A MO in the 5' untranslated region and/or surrounding the start codon prevents the development of a mature ribosome and scanning, and hence translation cannot occur. The MO can also block the formation of the mature ribosome if it is complementary to the start codon and extends into the coding sequence. However, if the MO binds too far downstream of the translation start site, the

mature ribosome forms and is able to translate the codons into proteins. In summary, translation-blocking MOs sterically hinder the translation initiation complex in order to prevent mRNA from being translated into protein.

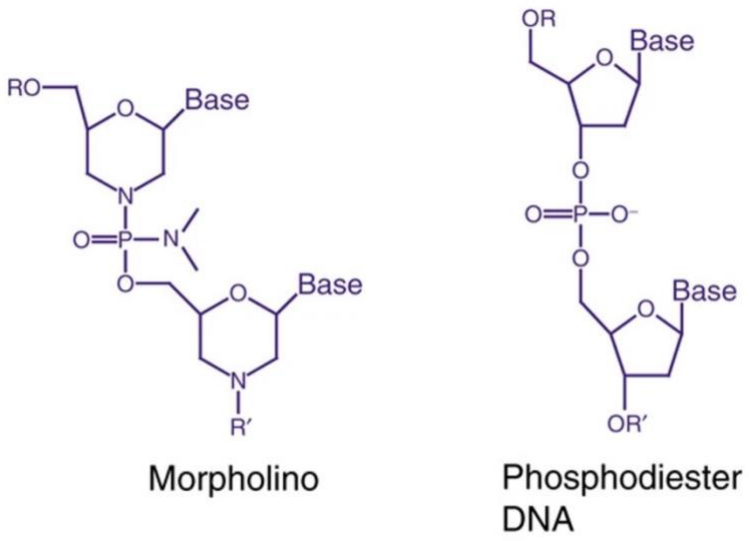

Figure 9. Comparison of MO and DNA structures. A MO is a single-stranded DNA analog comprised of morpholine rings and phosphorodiamidate linkages. A translation-blocking MO binds to its complementary sequence in the target mRNA and inhibits protein translation by steric blocking. As indicated by the letters R and R', the oligomer chain continues in either the 5' or 3' direction. Adapted from (Corey and Abrams, 2001).

Visualization of the MO is achieved by tagging the 3'-end of the oligo with various fluorophores, such as lissamine, which is a positively-charged and emits in the red channel. A 3′ lissamine-tagged translation-blocking Neurog2 MO (5′-TCTCCGCCTTCACCGGCATCC-3′), NeuroD1 MO (5'-CGGTGACGGTCGCATAACCCCG-3'), and a standard scrambled control MO prepared by the manufacturer (5′- CCTCTTACCTCAGTTACAATTTATA-3′), were designed to target their respective transcripts or serve as a control, respectively, according to the manufacturer's criteria (Gene Tools, LLC, Philomath, OR). All MOs were used at a concentration of 500 μM as previously described (Shah et al., 2017). As recommended by Gene Tools, the inverse complement of the MO sequence was compared with the chicken transcriptome using the NCBI Nucleotide BLAST tool to test the selected target for homologies with other transcripts. These results revealed that the designed MOs only base pair with *Neurog2* and *NeuroD1* transcripts and are not complementary to any other sites. Immunoblotting was also performed to demonstrate evidence of Neurog2 and NeuroD1 knockdown (see Section 2.8).

For electroporation, each MO was overlayed on top of the ectoderm of ~E1.5 (8-10ss) chick embryos (prior to placode cell delamination) by fine glass needles. After the MO was introduced, platinum electrodes were placed vertically across the chick embryo to deliver three pulses of 9 V, each lasting 50 milliseconds, at intervals of 200 milliseconds, as described (Shah et al., 2017). Eggs were re-sealed with tape and parafilm and incubation was then continued for ~18-24 hours until the embryos reached E2 (HH13-14). A Zeiss SteREO Discovery.V8 microscope and X-Cite Fluorescence illumination (series 120) was then used to screen the embryos *in ovo* for the presence of the red fluorescent signal that emanates from MO-positive cells in order to confirm that trigeminal placode cells had been electroporated. After screening, eggs were re-sealed and re-incubated for the desired time period.

2.3 Embedding and sectioning

Embryos were collected at the documented stages and rinsed in Ringer's solution (123 mM NaCl, 1.5 mM $CaCl_2$, 5 mM KCl, 0.8 mM Na_2HPO_4, 0.15 mM KH_2PO_4, pH 7.4). The embryos were then fixed via submersion and gentle shaking in 4% paraformaldehyde (PFA) overnight at 4°C, then permeabilized and rinsed three times in 1X phosphate-buffered saline (1X PBS) containing 0.1% Triton X-100 (0.1% PBST) for 10 minutes each. In order to prepare embryos for sectioning, fixed embryos were first immersed in 5% sucrose (w/v) in 1X PBS at room temperature for 10 minutes, or until the embryos sank, then in 15% sucrose at 4°C until the embryos sank. Embryos were then equilibrated in a solution of 15% sucrose and 7.5% gelatin for eight hours at 37°C and finally in 20% gelatin at 37°C overnight. After embryos were embedded in 20% gelatin with liquid nitrogen vapor, they were stored at -80°C until further use. Embryos were sectioned with a cryostat (Leica) at 12µm, and sections were collected on Superfrost Plus charged slides (VWR).

2.4 Trigeminal ganglion explant cultures

In a Sylgard-coated dish containing PB-1 standard medium, the forming trigeminal ganglion (ectoderm containing some trigeminal placode cells, placodal neurons, migratory neural crest cells, and cranial mesenchyme) was dissected using tungsten needles. Tissue was cultured in a two-well Lab-Tek II Chamber Slide (Thermo Fisher Scientific, 154461) coated with poly-L-lysine (Sigma-Aldrich, P5899) and fibronectin (Corning, 356008) containing serum-free DMEM (Corning, 10-013-CV) supplemented with 0.1% penicillin-streptomycin (10,000 U/ml; Gibco, MD; 15140122) and N-2 (Gibco, 17501-048) in a CO_2 incubator at 37°C (Basch et al.,

2006). These explant cultures formed trigeminal sensory neurons and were processed 48 hours after incubation as described below in Section 2.5.1.

2.5 Immunohistochemistry and tissue clearing

2.5.1 Tissue sections

Sectioned embryos were de-gelatinized and permeabilized with 0.1% PBST for 10 minutes at 42°C, blocked in 0.1% PBST and 10% sheep serum for at least 30 minutes at room temperature, and then rinsed once in 0.1% PBST. Primary antibodies were diluted in 0.1% PBST plus 5% sheep serum and applied overnight at 4°C in a humidified chamber. The following primary antibodies were obtained and used: Tubb3, 1:500, (Abcam, ab78078); DBN1, 1:100 (Thermo Fisher Scientific, PA5-34725); and STMN2, 1:250 (Thermo Fisher Scientific, 720178). Unbound primary antibodies were washed off with four rinses of 0.1% PBST for 30 minutes each at room temperature. Sections were then incubated with secondary antibodies diluted in 0.1% PBST plus 5% sheep serum, for two to three hours at room temperature, or overnight at 4°C in a humidified chamber. The following secondary antibodies were obtained and used at a 1:250 dilution: Goat anti-mouse IgG_{2a} AlexaFluor 488 or 647 (Southern Biotech, 1080-30 or 1080-31, for Tubb3) or goat anti-rabbit IgG Alexa Fluor 488 (Thermo Fisher Scientific, A11034, for DBN1 and STMN2). Sections were rinsed four times in 0.1% PBST for 30 minutes each at room temperature. To mark cell nuclei, coverslips were mounted with DAPI-containing Fluoromount-G Mounting Medium (Southern Biotech), which was allowed to dry in the dark at room temperature overnight before imaging. For E2.5-3 (HH16-18) embryos, a minimum of five serial sections from at least five embryos were examined for Tubb3 immunoreactivity as described above.

2.5.2 Whole embryo

Fixed embryos in 4% PFA were rinsed and then blocked in 0.1% PBST and 10% sheep serum for two hours at room temperature. Afterwards, the embryos were rinsed three times in 0.1% PBST for 10 minutes each. Embryos were then incubated overnight at 4°C with fresh antibody dilution solution containing primary antibody (Tubb3, 1:300) in 0.1% PBST and 5% sheep serum, with gentle shaking. Next, embryos were washed four times for 30 minutes each at room temperature with 0.1% PBST, then incubated in fresh dilution solution with secondary antibody (goat anti-mouse IgG_{2a} AlexaFluor 488, 1:250) overnight at 4°C with gentle shaking. Embryos were washed four times for 30 minutes each at room temperature with 0.1% PBST. Embryos were cleared before imaging, as described below.

2.5.3 Fructose and urea solution (FRUIT) clearing

Following immunohistochemistry, embryos were cleared via FRUIT, which utilizes a cocktail of fructose and urea to achieve maximum transparency of tissue without deformation (Hou et al., 2015). Embryos were incubated in a series of FRUIT buffer solutions containing 8M urea (Millipore Sigma), 0.5% (v/v) α-thioglycerol (TCI America), and increasing amounts of fructose (Millipore Sigma). Embryos were gently rocked in 35% FRUIT for six hours, 40% FRUIT for eight hours, 60% FRUIT for eight hours, and 80% FRUIT overnight, with all incubations carried out at room temperature. Embryos were kept at 4°C in 80% FRUIT before imaging.

2.6 Terminal deoxynucleotidyl transferase dUTP nick end labeling (TUNEL) staining

TUNEL staining was conducted after immunohistochemistry on tissue sections using the *In Situ* Cell Death Detection Kit, Fluorescein (Roche) as directed by the manufacturer. Following removal of unbound secondary antibodies, slides were post-fixed with 4% PFA in 1X PBS at room temperature for 20 minutes, then washed twice with 1X PBS for five minutes each at room temperature. After incubation for one hour in a humidified chamber at 37°C in the dark with TUNEL reaction mixture, sections were washed at room temperature in 1X PBS twice for 10 minutes each. DAPI-containing Fluoromount-G Mounting Medium was used to mount the cover slips (and label cell nuclei) before imaging. The coverslips were then allowed to dry in the dark at room temperature.

2.7 Confocal imaging

Embryos were imaged in 80% FRUIT buffer on a Zeiss LSM 800 confocal microscope and Z-stacks were collected using 5X or 10X air objectives. The same microscope was also used to image fluorescent immunohistochemistry results from tissue sections using air objectives at 5X, 10X, and 20X, or an oil objective at 40X. When using contralateral control versus electroporated sides to image comparable regions of interest, laser power, gain, offset, and digital zoom were kept the same in each application, and the pinhole was always set to one airy scan unit. Zen software (Blue edition 2.0, Zeiss) was then used to process the CZI files. For Z-stacks, the CZI files were processed in ImageJ, and the Z-Project function in HyperStack mode was used to create maximum intensity projections.

2.8 Immunoblotting

The knockdown efficiencies of both Neurog2 and NeuroD1 MOs were evaluated by collecting and pooling electroporated trigeminal ganglia dissected from Neurog2- (n = 25), NeuroD1- (n = 17), and control MO- (n = 25, n = 22, respectively) treated embryos at E2.5-3 (HH16-18). Samples were rinsed in Ringer's solution, centrifuged at 500 g for five minutes at 4°C, and then snap-frozen in liquid nitrogen. Cell pellets were lysed in lysis buffer (50 mM Tris-HCl pH 8.0, 100 mM NaCl, 0.5% IGEPAL CA-630, 1 mM EDTA) supplemented with cOmplete™ Mini Protease Inhibitor Cocktail (Roche) and 1 mM PMSF (Sigma-Aldrich) for 30 minutes at 4°C with mixing every 10 minutes. Following centrifugation at >20,000 g for 15 minutes at 4°C, the clarified, solubilized protein fraction was collected, and protein concentration was calculated using the Bradford assay (Thermo Fisher Scientific). Each sample (containing equivalent amounts of protein) was boiled at 95°C for five minutes in 1X reducing Laemmli sample buffer and then centrifuged at maximum g for five minutes at room temperature. The samples were then loaded onto a 14% SDS-PAGE gel, separated by electrophoresis, and subsequently transferred to a 0.45 μm BioTrace PVDF membrane (Pall, Port Washington, NY). Membranes were incubated in blocking solution (1X PBS and 0.1% Tween (PTW) + 5% dry milk) for one hour at room temperature and then incubated overnight at 4°C with the following primary antibodies diluted in blocking solution: Neurog2 (1:200, Santa Cruz Biotechnology, sc-293430) and NeuroD1 (1:1000, Life Science Biotechnology, LS-C331294). Membranes were washed three times in PTW for 10 minutes each and then incubated with species- and isotype-specific horseradish peroxidase-conjugated secondary antibodies at 1:15,000 dilution (Neurog2: mouse IgG-HRP, Rockland, 610-1302; NeuroD1: rabbit IgG-HRP, Rockland, 611-1302) in blocking solution for one hour at room temperature. PTW washes were repeated three times for

10 minutes each, and chemiluminescent substrates (Supersignal West Pico or Femto, Thermo Fisher Scientific), along with a ChemiDoc XRS system (Bio-Rad), were used for detection. The immunoblots were then stripped using Restore Plus western blot stripping buffer (Thermo Fisher Scientific) for 15 minutes at 37°C and re-probed with a loading control antibody (anti-Beta-actin primary antibody (1:1,500, Santa Cruz Biotechnology, sc-47778, for the Neurog2 blot); anti-GAPDH primary antibody (1:10,000, Thermo Fisher Scientific, MA5-15738) for the NeuroD1 blot), followed by their species- and isotype-specific secondary antibodies (mouse IgG-HRP, 1:15,000, Rockland, 610-1302). Immunoblots were analyzed using Image Lab software (Bio-Rad) in order to determine band size and volume.

Results

Chapter 3: Evaluating the role of Neurog2 in trigeminal ganglion growth and development

A vertebrate's remarkable ability to sense the environment can be attributed to paired sensory organs (olfactory epithelium, inner ear, and eye), the cranial nerves, and their associated sensory ganglia. Each of these develops from ectodermal placodes during embryogenesis, with the exception of the eye. Interactions between neural crest cells and placode cells are critical to coordinate the development of these ganglia during vertebrate craniofacial development (Steventon et al., 2014). The process by which proliferative and multipotent neural precursors become fully differentiated neurons is called neurogenesis (Urbán and Guillemot, 2014). Neurogenesis relies on many proteins working together, and therefore their activities must be tightly regulated. Transcription factors in the bHLH family control commitment of progenitor cells to specific fates in neural development (Powell and Jarrman, 2008). Previously published findings indicated that bHLH transcription factors are essential in neurogenesis (Baker and Bronner-Fraser, 2001; Powell and Jarrman, 2008; Bronner and Simões-costa, 2016).

Neurog2 is a bHLH transcription factor that is expressed from ~E1.5 (HH10) onward in chick embryos. Moreover, it is an ophthalmic placode-specific marker until E2.5 (HH16) (Xu et al., 2008), after which it is considered a marker for all placode-derived neurons since its expression is detected in other placodes at E2 and in the maxillomandibular neurons of the trigeminal ganglion at E3 (HH18) (Xu et al., 2008). Prior research has shown that *Neurog1* and *Neurog2* knockout in mice prevents trigeminal (Ma et al., 1998) and epibranchial (Fode et al., 1998) ganglion development, respectively. The expression of *Neurogs* in the neurogenic placodes of the chick differs from that of the mouse, though, with *Neurog2* expression confined

to the ophthalmic trigeminal placodes in the chick (Begbie et al., 2002). However, its function in the development of the chick trigeminal ganglion is largely unknown.

Given these findings and gap in knowledge, the first aim of this study was to investigate the role of Neurog2 in regulating trigeminal ganglion development. To examine the function of Neurog2 during trigeminal ganglion neurogenesis, Neurog2 knockdown experiments were carried out in trigeminal placode cells followed by immunohistochemistry on whole embryos and sections. Our results indicated that depletion of Neurog2 in trigeminal placode cells impaired trigeminal ganglion development, leading to the apparent reduction in placode-derived neurons within the trigeminal ganglion. This decrease in ganglion size was likely not due to increased apoptosis, at least at the examined stages. However, Neurog2 knockdown may affect neural crest-derived neurons at later stages of development due to the reciprocal interactions between placode cells and neural crest cells. These data shed new light on the molecular mechanisms underlying trigeminal gangliogenesis and may lead to an in-depth understanding of diseases of the nervous system.

3.1 The Neurog2 MO is effective in reducing Neurog2 protein levels.

In order to knockdown Neurog2 expression, a MO was designed to target the sequence surrounding the start site of the *Neurog2* transcript (Figure 10; see Chapter 2 for more details). The Neurog2 MO, or a standard scrambled control MO (from GeneTools, LLC; hereafter referred to as control MO), was overlayed on top of the chick ectoderm, followed by unilateral ectodermal electroporation. To ensure that the embryo was electroporated with MO, embryos were screened *in ovo* ~12 hours post-electroporation. The embryos were re-incubated for a

specified period of time, and then processed to examine the effect of knockdown on trigeminal ganglion development, and specifically the contribution of placode cells.

The efficacy of the Neurog2 MO was tested by electroporating either the control MO or the Neurog2 MO, followed by collection of electroporated trigeminal ganglia at E2-3 to examine Neurog2 protein levels by immunoblotting (Shah et al., 2017). Analysis of Neurog2 protein revealed a 30% reduction in the presence of the Neurog2 MO compared to the control MO (Figure 11).

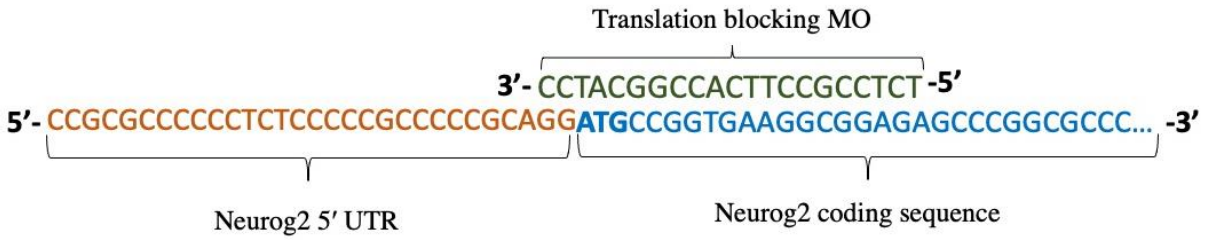

Figure 10. The Neurog2 MO inhibits translation of *Neurog2* transcripts. This translation-blocking MO works by preventing translation initiation complexes from reaching the *Neurog2* start codon. Abbreviation: UTR, untranslated region.

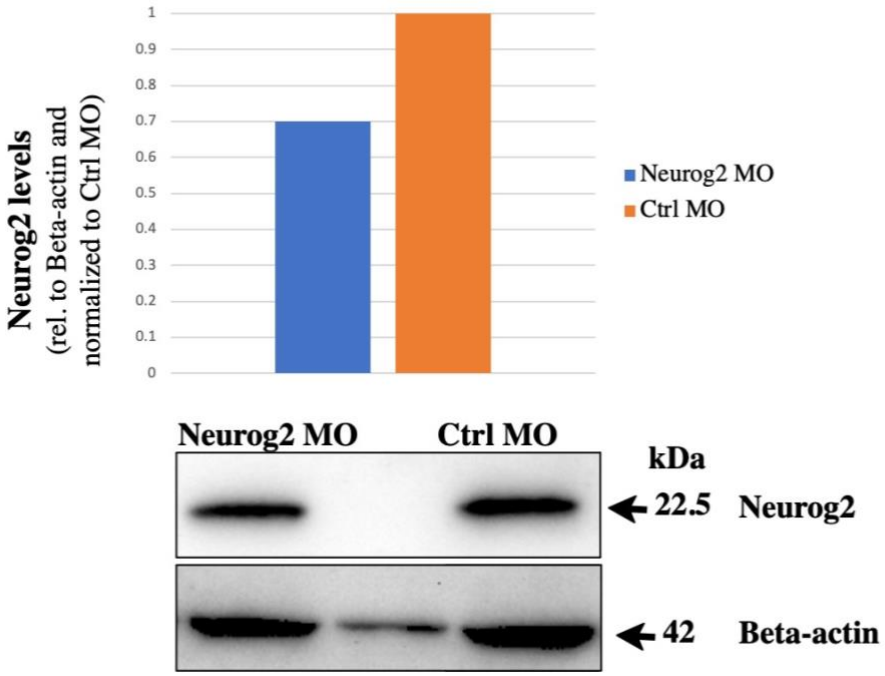

Figure 11. The Neurog2 MO reduces Neurog2 protein levels by 30%. At ~E1.5 (HH9^{+} to 10), placode cells were unilaterally electroporated either with a Neurog2 or control (Ctrl) MO. After re-incubation to E2.5-3 (HH16-18), the forming trigeminal ganglion on the electroporated side was dissected and pooled from multiple embryos. Lysates were prepared, and equivalent amounts of protein per sample were separated on a 14% SDS-PAGE gel. Immunoblotting for Neurog2 and Beta-actin (control) was then performed, and band intensity was calculated from unmodified immunoblot images using Image Lab software (Bio-Rad). Relative protein levels were ascertained by normalizing Neurog2 volumes to B-actin volumes. Knockdown amount was determined by comparing normalized ratios between Ctrl MO and Neurog2 MO samples, with the Ctrl MO sample set as one. On the B-actin panel, an extra band is present corresponding to lysate spillover from adjacent lanes.

3.2 Knockdown of Neurog2 in trigeminal placode cells leads to abnormalities in trigeminal ganglion development.

After unilateral electroporation of Neurog2 MO using methods described in #3.1 above, the embryos were re-incubated to E3-5 (HH18-26), collected, fixed, and processed for whole-mount immunohistochemistry to detect Beta-tubulin III (Tubb3), which labels differentiated neurons in the developing ganglion. Neuronal differentiation at E2.5-3.5 (HH16-21) occurs mostly in the placodal population while neural crest cells begin to differentiate into neurons starting at E4 (HH22-24) (Hamburger, 1961; D'Amico-Martel and Noden, 1980; Shiau et al., 2008). Thus, both neural crest- and placode-derived neurons are labeled with this antibody, depending upon the developmental stage. Confocal images of whole embryo heads were obtained to examine gross trigeminal ganglion morphology. Trigeminal ganglion morphology on the electroporated side was then compared to that on the contralateral control side, which possessed no MO (Figure 12-14).

At E3 (HH18) (Figure 12), drastic changes in the trigeminal ganglion are already apparent. In contrast to the contralateral control side (Figure 12A), the entire trigeminal ganglion and associated nerve structures were diminished in size on the Neurog2-depleted side (Figure 12B). Moreover, neurons in the ophthalmic branch did not innervate the eye region properly (Figure 12B, arrowheads). In addition, knockdown of Neurog2 may impede segregation of the maxillomandibular branch into definitive maxillary and mandibular branches, as shown by neurons deviating from the established maxillary branch (Figure 12A, B, D, E, carets). Besides these observations, however, the general morphology of the ganglion appeared similar: a bilobed structure possessing ophthalmic and maxillomandibular branches. Although Tubb3-positive

placodal neurons can be observed throughout the forming ganglion, higher magnification images (Figure 12D-F) revealed neurons that were less organized and seem to drift away from established axon bundles. Axons of the maxillomandibular nerve also traveled without direction from the established nerve in the Neurog2-depleted side (Figure 12E) compared to the contralateral control side (Figure 12D).

At E3-3.5 (HH20), the trigeminal ganglion and associated nerve structures were still reduced in size after Neurog2 knockdown (Figure 13B) compared to the untreated contralateral control side (Figure 13A). Furthermore, the ophthalmic nerve extended less elaborately around the eye than on the contralateral control side (Figure 13A, B, arrowheads). Maxillary neurons were arranged in bundles but appeared less compact after Neurog2 knockdown than on the untreated side (Figure 13A, B, carets). However, both the electroporated and contralateral control sides appeared to have similar overall morphology with respect to the ganglion and its branches. With higher magnification (Figure 13D-F), though, a reduction in the size of the ophthalmic nerve, and presence of likely fewer placode-derived neurons, were better appreciated (Figure 13D, E, brackets).

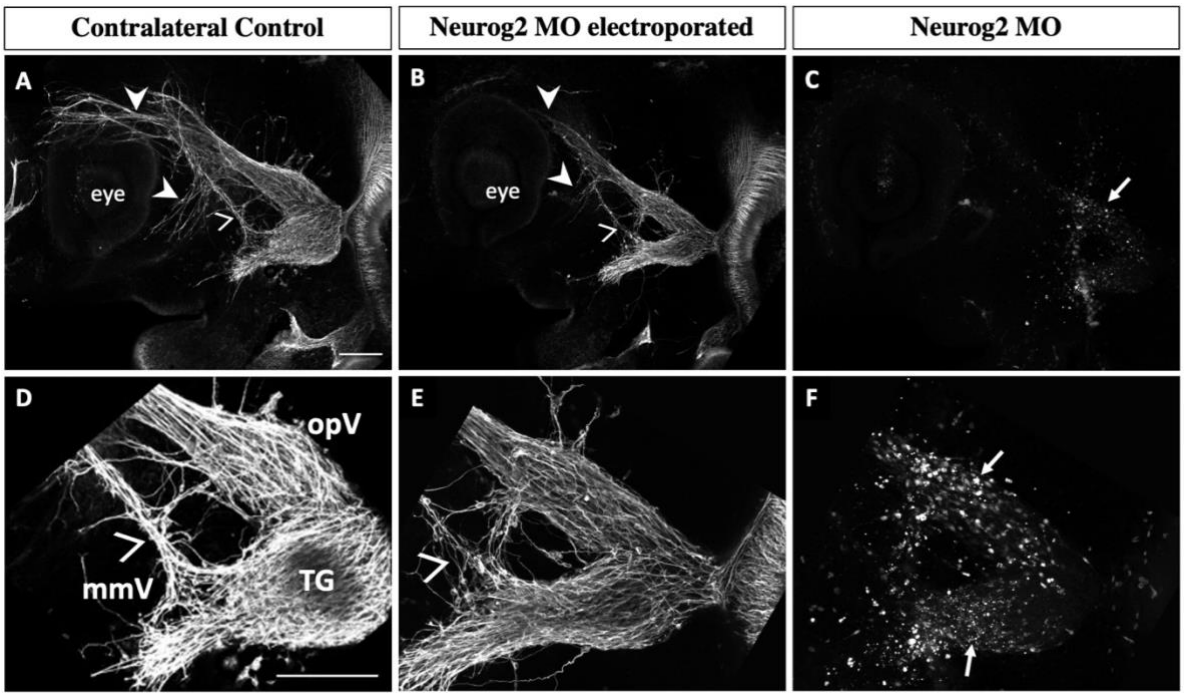

Figure 12. Depletion of Neurog2 in trigeminal placode cells impairs trigeminal ganglion development. Lateral view of the trigeminal ganglion in a chick head (E3 (HH18), n = 4). Representative images are maximum intensity projections of confocal Z-stacks through the contralateral control (A, D) and Neurog2 MO electroporated (B, E) side after processing for whole-mount Tubb3 immunohistochemistry to detect placode-derived neurons (A, B, D, E, arrowheads) and tissue clearing. Bottom row shows higher magnification images of the top row. (C, F) MO-positive cells (arrows). Scale bar is 1mm (A, D) and applies to all images. Abbreviations: mmV, maxillomandibular lobe; opV, ophthalmic lobe; TG, trigeminal ganglion.

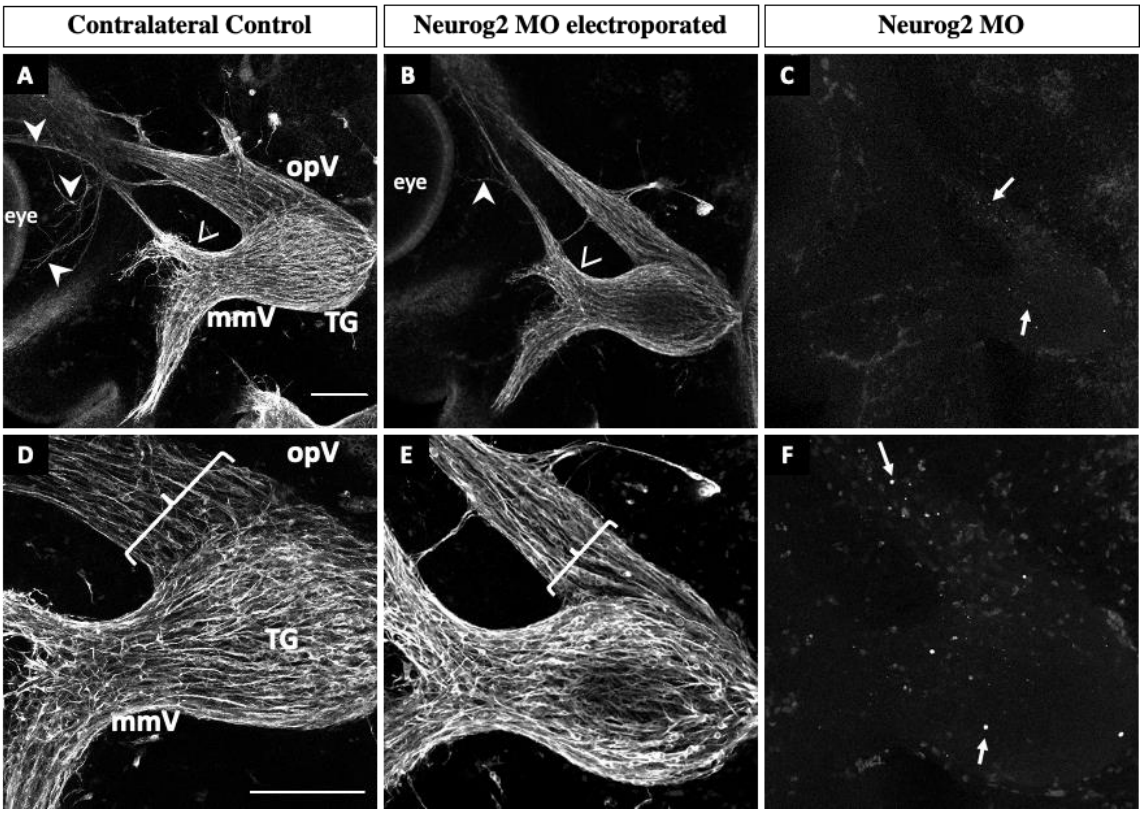

Figure 13. Neurog2 depletion in trigeminal placode cells disrupts trigeminal ganglion development. Lateral view of the trigeminal ganglion in a chick head (E3-3.5 (HH20), n = 5). Representative images are maximum intensity projections of confocal Z-stacks through the contralateral control (A, D) and Neurog2 MO electroporated (B, E) side after processing for whole-mount Tubb3 immunohistochemistry to detect placode-derived neurons (A, B, D, E, arrowheads) and tissue clearing. Bottom row shows higher magnification images of the top row. (C, F) MO-positive cells (arrows). Brackets indicate width of ophthalmic branch. Scale bar is 200μm (A, D) and applies to all images. Abbreviations: mmV, maxillomandibular lobe; opV, ophthalmic lobe; TG, trigeminal ganglion.

Although Tubb3 immunoreactivity was weaker at E5 (HH26) (Figure 14), likely due to poor penetration of the antibody into the whole embryo head, defects were still observed in the Neurog2 MO-electroporated trigeminal ganglion and its branches (Figure 14B, arrowhead) compared to the same structures on the contralateral control side (Figure 14A, arrowhead). At this stage, neural crest cells have also differentiated into neurons so Tubb3 identifies both placode- and neural crest-derived neurons. These results reveal that Neurog2 knockdown primarily impacted the development of the ophthalmic branch of the trigeminal ganglion since the ophthalmic branch is drastically smaller and appears to contain fewer neurons compared to the contralateral control side of the embryo (Figure 14A, B, brackets).

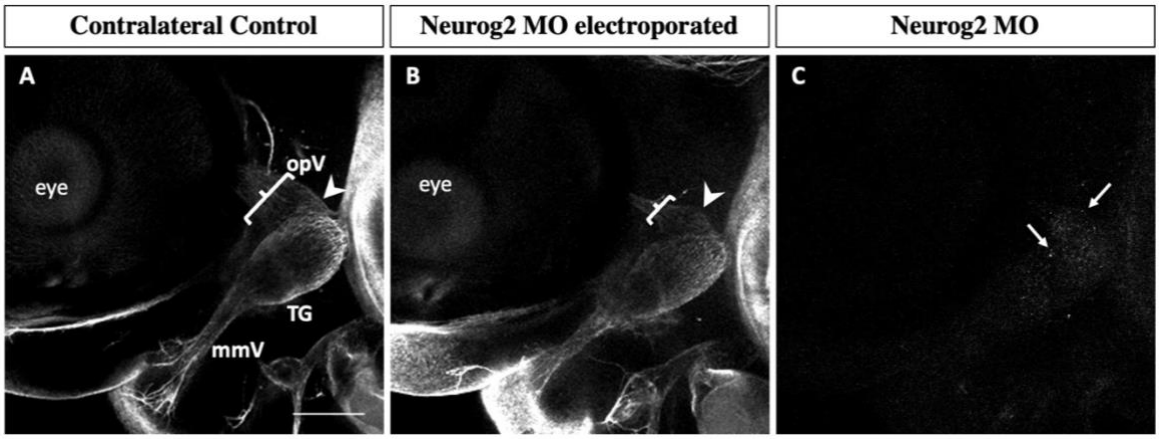

Figure 14. Neurog2 depletion in the trigeminal placode cells impedes trigeminal ganglion development. Lateral view of the trigeminal ganglion in a chick head (E5 (HH26), n = 3). Representative images are maximum intensity projections of confocal Z-stacks through the contralateral control (A) and Neurog2 MO electroporated (B) side after processing for whole-mount Tubb3 immunohistochemistry to detect placode-derived neurons (A, B, arrowheads) and tissue clearing. MO-positive cells (C, arrows). Brackets indicate width of ophthalmic branch. Scale bar is 500μm in (A) and applies to all images. Abbreviations: mmV, maxillomandibular lobe; opV, ophthalmic lobe; TG, trigeminal ganglion.

3.3 Neurog2 knockdown in trigeminal placode cells decreases the size of the trigeminal ganglion ophthalmic lobe.

We examined the morphology of the trigeminal ganglion after Neurog2 depletion over the course of development. After knockdown of Neurog2 using methods described in #3.1 above, embryos were re-incubated to E2-4.5 (HH15-24). To evaluate the distribution of neurons within the ganglion, the embryos were then sectioned and processed for immunohistochemistry using Tubb3, which, at these stages, labels placode-derived neurons.

A representative cross-section of an embryo through the forming ophthalmic lobe of the trigeminal ganglion is shown at lower magnification at ~E2 (HH15) (Figure 15A-C). A number of placodal neurons, many of which are MO-positive, were found in the ganglionic anlage on the electroporated side. Overall, the ganglion morphology appeared to be similar on both sides, but subtle differences were observed. As noted at a higher magnification on the electroporated side, forming trigeminal neurons were more dispersed (Figure 15G, arrowheads) compared to those seen on the contralateral control side (Figure 15D). Moreover, many electroporated placode cells (Figure 15I) successfully differentiated into neurons and delaminated from the ectoderm to migrate to the ganglion-forming region (Figure 15H, arrows), where they will intermingle with neural crest cells (not shown).

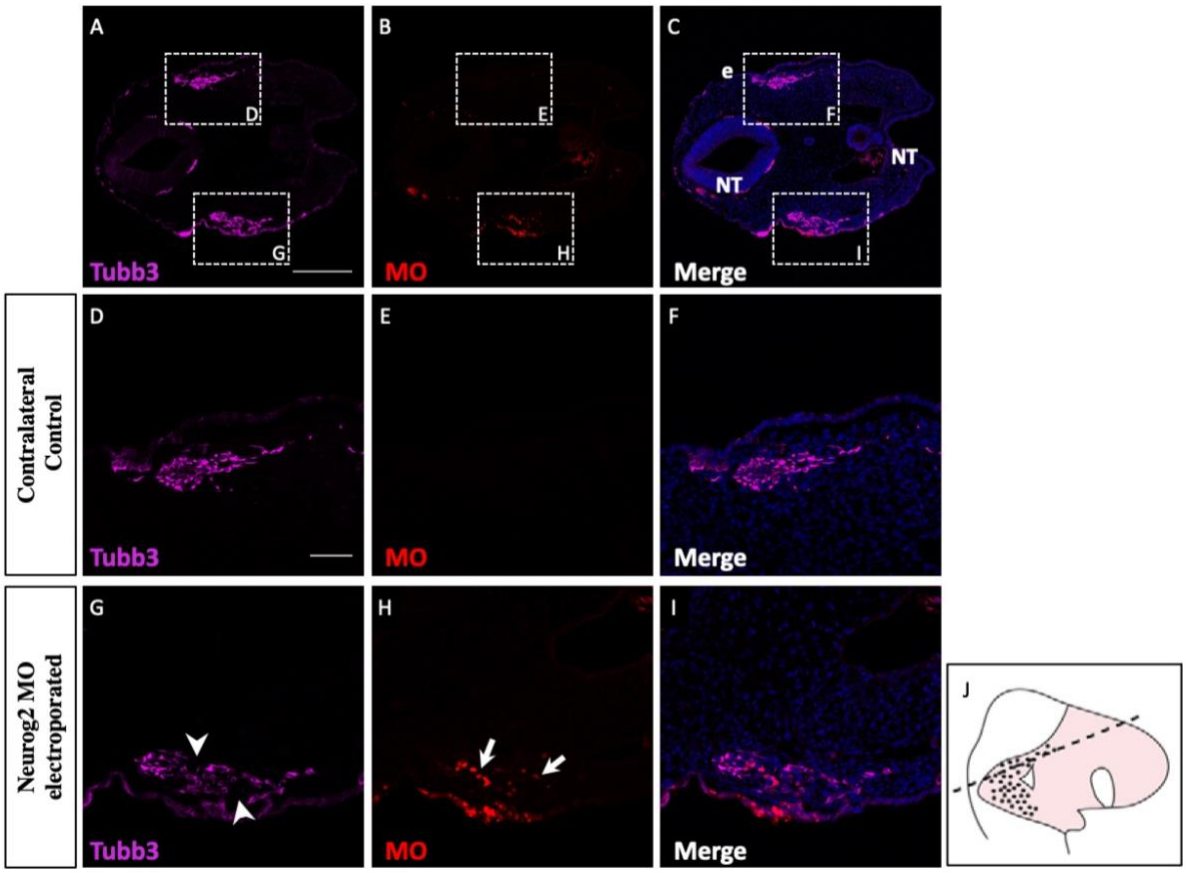

Figure 15. Trigeminal ganglion development is impaired by Neurog2 depletion in trigeminal placode cells. Representative transverse section through the forming trigeminal ganglion (~E2 (HH15), n = 3) after Neurog2 MO unilateral electroporation (B, E, H, red, arrows) followed by Tubb3 immunohistochemistry to detect placode-derived neurons (A, C, D, F, G, I, purple, arrowheads). Boxed regions in (A-C) are shown at higher magnification for the contralateral (D-F) and Neurog2 MO-electroporated (G-I) sides. (J) Cartoon diagram of the developing chick developing trigeminal ganglion with dashed line indicating its section plane (A to I), adapted from (Shiau and Bronner-Fraser, 2009). DAPI (blue), cell nuclei. Scale bar is 200μm in (A) and applies to (B, C) and 50μm in (D) and applies to (E-I). Abbreviations: e, ectoderm; NT, neural tube.

At ~E2.5 (HH17), a cross-section through the ophthalmic branch uncovered that the trigeminal ganglion was much smaller on the Neurog2 MO-electroporated side after an additional 12 hours of development (Figure 16A-C). At higher magnification (Figure 16D-I), it was evident that the ganglion possesses many MO-positive cells (Figure 16H, arrows), indicating that many of the electroporated cells have delaminated and migrated from the ectoderm to coalesce with neural crest cells (not shown) and form the trigeminal ganglion. However, fewer placodal neurons appeared to be present in the trigeminal ganglion after Neurog2 knockdown (Figure 16G, arrowhead) compared to the contralateral control side (Figure 16D).

At E4.5 (HH24), Neurog2 knockdown still resulted in a smaller trigeminal ganglion compared to the contralateral control side of the embryo (Figure 17A-C). Additionally, in higher magnification images (Figure 17D-I), some MO-negative neurons appeared less condensed (Figure 17G, arrowheads), which could be placodal neurons that are not electroporated or neural crest-derived neurons. Therefore, Neurog2 knockdown may negatively affect the size of the trigeminal ganglion by possibly influencing the assembly of neurons within the ganglion.

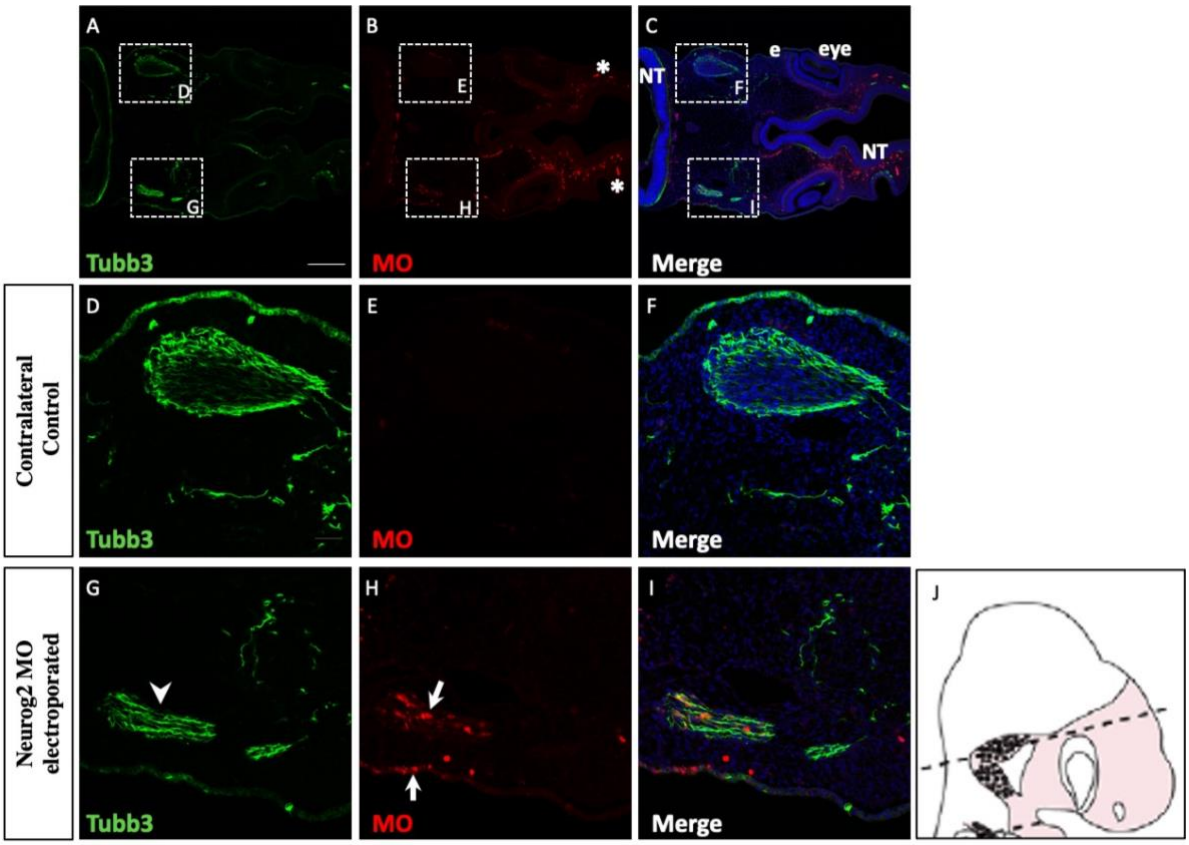

Figure 16. Neurog2 knockdown in trigeminal placode cells decreases the size of the trigeminal ganglion ophthalmic lobe. Representative transverse section through the forming trigeminal ganglion (~E2.5 (HH17), n = 3) after Neurog2 MO unilateral electroporation (B, E, H, red, arrows) followed by Tubb3 immunohistochemistry to detect placode-derived neurons (A, C, D, F, G, I, green, arrowhead). Boxed regions in (A-C) are shown at higher magnification for the contralateral (D-F) and Neurog2 MO-electroporated (G-I) sides. Asterisks mark red blood cells (B). (J) Cartoon diagram of the developing chick developing trigeminal ganglion with dashed line indicating its section plane (A to I), adapted from (Shiau and Bronner-Fraser, 2009). DAPI (blue), cell nuclei. Scale bar is 1mm in (A) and applies to (B, C) and 200μm in (D) and applies to (E-I). Abbreviations: e, ectoderm; NT, neural tube.

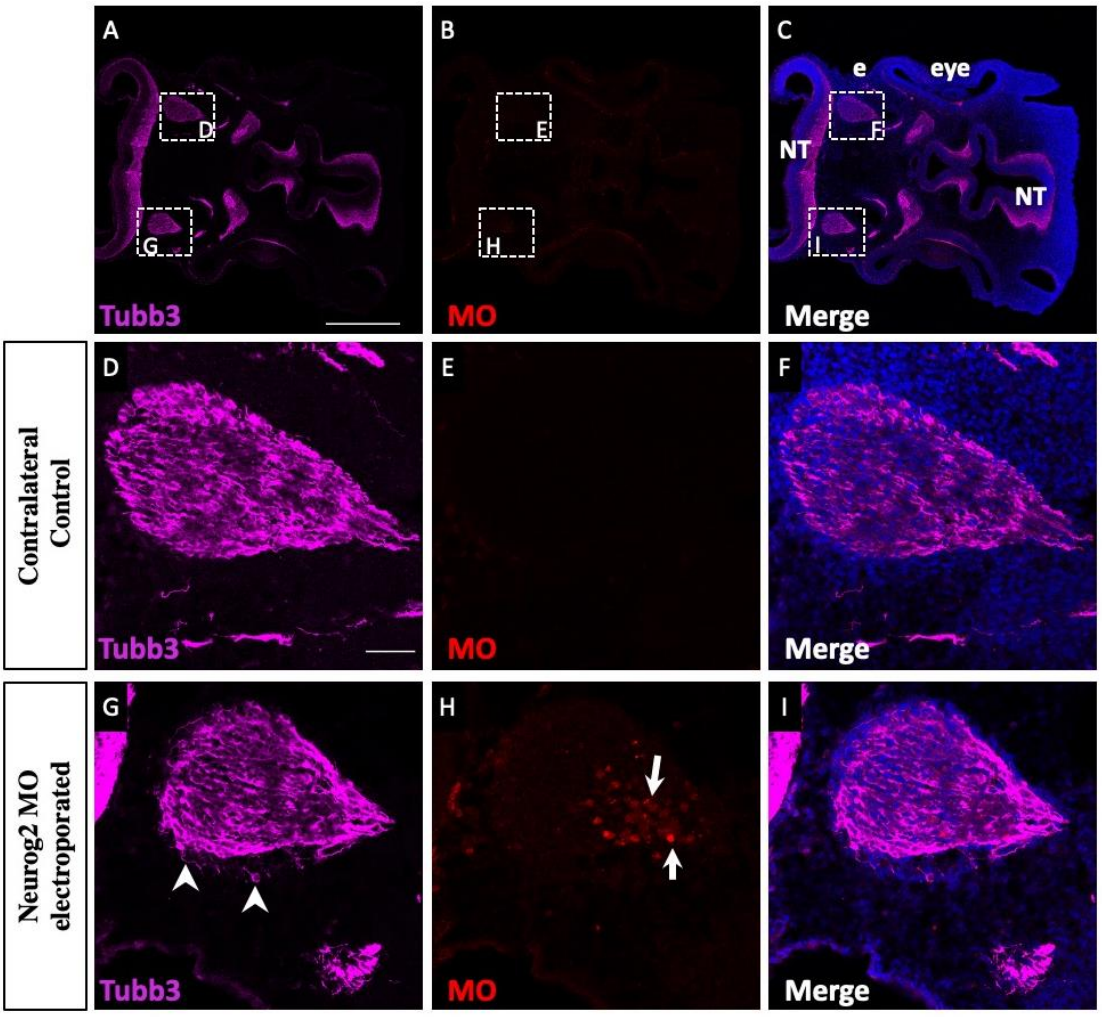

Figure 17. Neurog2 knockdown in trigeminal placode cells decreases the size of the trigeminal ganglion ophthalmic lobe. Representative transverse section through the forming trigeminal ganglion (E4.5 (HH24), n = 1) after Neurog2 MO unilateral electroporation (B, E, H, red, arrows) followed by Tubb3 immunohistochemistry to detect placode-derived neurons (A, C, D, F, G, I, purple, arrowheads). Boxed regions in (A-C) are shown at higher magnification for the contralateral (D-F) and Neurog2 MO-electroporated (G-I) sides. DAPI (blue), cell nuclei. Scale bar is 500μm in (A) and applies to (B, C) and 50μm in (D) and applies to (E-I). Abbreviations: e, ectoderm; NT, neural tube.

3.4 Neurog2 depletion does not cause apoptosis of trigeminal placode cells or their neuronal derivatives during initial trigeminal ganglion assembly.

Next, we investigated whether the phenotype observed in #3.2 and #3.3 (smaller trigeminal ganglion) was due to increased cell death caused by Neurog2 knockdown. To this end, we performed TUNEL analyses at ~E2 (HH15) to detect apoptotic cells after unilateral electroporation of trigeminal placode cells with Neurog2 MO earlier in development. Neurog2 knockdown (Figure 18D-F) did not lead to apoptosis of MO-positive cells, and, qualitatively, there was no general change in the number of apoptotic cells compared to the contralateral control side (Figure 18A-C). These results indicate that depletion of Neurog2 from placode cells does not lead to increased cell death in the trigeminal ganglion at this developmental stage.

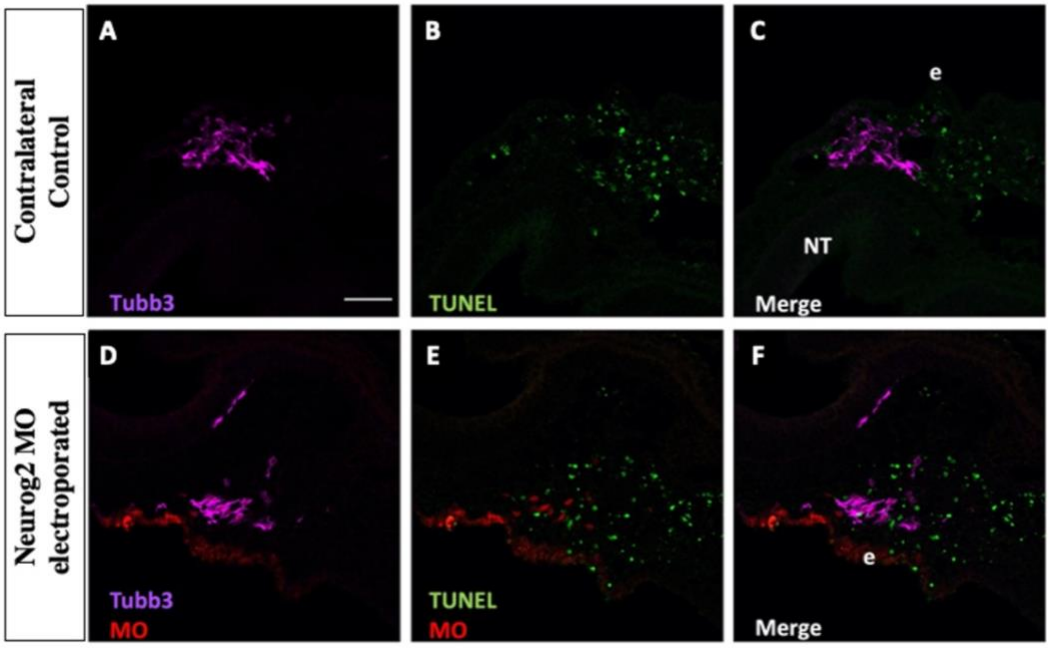

Figure 18. Depletion of Neurog2 in trigeminal placode cells does not cause increased cell death. Representative transverse section through the forming trigeminal ganglion (~E2 (HH15), n = 1) after Neurog2 MO unilateral electroporation (D, E, F, red) followed by Tubb3 immunohistochemistry to detect placode cell-derived neurons (A, C, D, F, purple) and TUNEL staining to identify apoptotic cells (B, C, E, F, green). Scale bar in (A) is 200μm and applies to all images. Abbreviations: e, ectoderm; NT, neural tube.

Despite achieving only 30% reduction in Neurog2 protein levels, Neurog2 MO treatment clearly caused dramatic effects on trigeminal gangliogenesis, providing evidence that this protein is important for trigeminal ganglion development. These findings are consistent with previous reports showing loss of the trigeminal, and geniculate and petrosal, ganglia in *Neurog1* and *Neurog2* knockout mouse embryos, respectively (Ma et al., 1998). Higher knockdown efficiency may have more serious consequences, such as a complete loss of the trigeminal ganglion, severe craniofacial abnormalities, or even death of the developing embryo. On the basis of the stages examined, Neurog2 promotes trigeminal gangliogenesis and effective target innervation, specifically in the ophthalmic branch (Figures 12-17). *Neurog2* is exclusively expressed by the ophthalmic trigeminal placode in chick embryos from ~E1.5 (HH10) onward, and is detected in other placode cells later in development at E2.5 (HH16) and in maxillomandibular neurons at E3 (HH18). Thus, knockdown of Neurog2 in the trigeminal placode may not have the same profound effect on maxillomandibular neurons as it does on ophthalmic neurons. Considering the high degree of interaction between neural crest and placode cells during ganglion assembly, the dispersal of potentially neural crest-derived neurons at later stages of development is not surprising (Figure 17G). Alternatively, since electroporation is not 100% effective, there may be placode-derived neurons that are not electroporated but still show defective coalescence in the ganglion due to a general effect on trigeminal ganglion formation after Neurog2 knockdown. In the following chapter, we examine the effects of knockdown of NeuroD1, a downstream target of Neurog2, in trigeminal placode cells on the development of the trigeminal ganglion and placodal neurons.

Chapter 4: Investigating the role of NeuroD1 in trigeminal gangliogenesis

The bHLH protein family is an important class of transcription factors that activates gene expression in a wide range of processes essential to development including cell type determination (Lee et al., 1995). The bHLH transcription factor NeuroD1 has been reported to be downstream of Neurog2 in various cell types, including the mouse embryonic epibranchial placodes (Fode et al., 1998; Ma et al., 1998) and in *Xenopus* multi-potent naive ectodermal explants (Seo et al., 2007). Transcriptional regulation is stimulated by direct binding of NeuroD1 to regulatory elements of neuronal development genes, resulting in the recruitment of downstream transcription factors that regulate gene expression and promote neurogenesis (Pataskar et al., 2016; Singh et al., 2022). In addition to its role in neurogenesis, NeuroD1 also plays a key function in migration, maturation, and survival of newborn neurons (Singh et al, 2022). Knocking down *NeuroD1* in human pluripotent stem cells induced to differentiate into neurons impaired their ability to become bipolar neurons, implicating NeuroD1 in the control of neuronal morphology during maturation (Busskamp et al., 2014).

NeuroD1 is widely expressed in the chick embryo placodal ectoderm before delamination and persists in the placode-derived cranial ganglia until E8 (Abu-Elmagd et al., 2001). Although prior studies have characterized NeuroD1 expression and function, as indicated above, the role of NeuroD1 in the chick trigeminal ganglion remains poorly understood. Therefore, the second aim of this study was to investigate the role of NeuroD1 in regulating trigeminal ganglion development. To address this aim, NeuroD1 knockdown experiments were carried out in trigeminal placode cells followed by immunohistochemistry on whole embryos and sections. Depletion of NeuroD1 in trigeminal placode cells negatively affected trigeminal ganglion

development, likely due to a reduction in placode-derived neurons within the ganglion and a decrease in ganglion size. There is also the possibility that neural crest-derived neurons are adversely affected after NeuroD1 knockdown due to the reciprocal interactions required between placode cells and neural crest cells during trigeminal ganglion formation. Our data have shed light on the molecular events that regulate trigeminal ganglion formation and contribute to our understanding of the neuropathology of the peripheral nervous system.

4.1 The NeuroD1 MO effectively reduces NeuroD1 protein levels.

In order to knockdown NeuroD1 expression, a MO was designed to target the sequence surrounding the start site of the *NeuroD1* transcript (Figure 19; see Chapter 2 for more details). At ~E1.5 after placode cell specification but prior to delamination from the ectoderm, the NeuroD1 MO, or a control MO (from GeneTools, LLC), was overlayed on top of the chick ectoderm, followed by unilateral ectodermal electroporation. The embryos were screened ~12 hours after electroporation to ensure they had been electroporated with MO. Incubation of the embryos for a specified period of time was followed by immunohistochemistry in order to examine the effects of knockdown on trigeminal ganglion development, specifically focusing on the role of placode cells.

We first tested the efficacy of the NeuroD1 MO by evaluating NeuroD1 protein levels through immunoblotting (Shah et al., 2017). To this end, trigeminal placode cells were electroporated with either a control MO or the NeuroD1 MO. Electroporated trigeminal ganglia at E2.5-3 (HH16-18) were then dissected and pooled for immunoblotting, which revealed two different bands immunoreactive with the NeuroD1 antibody and corresponding to NeuroD1 protein (Figure 20). Both bands are reduced in intensity after MO-mediated knockdown of

NeuroD1. Compared to NeuroD1 protein in the control MO sample, knockdown of NeuroD1 via the MO resulted in a 55% and 63% decrease in the 50 kDa and 47 kDa NeuroD1 protein bands, respectively.

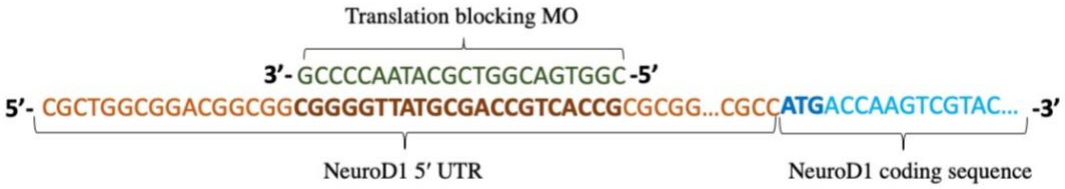

Figure 19. The NeuroD1 MO inhibits translation of *NeuroD1* transcripts. This translation-blocking MO works by preventing translation initiation complexes from reaching the *NeuroD1* start codon. Abbreviation: UTR, untranslated region.

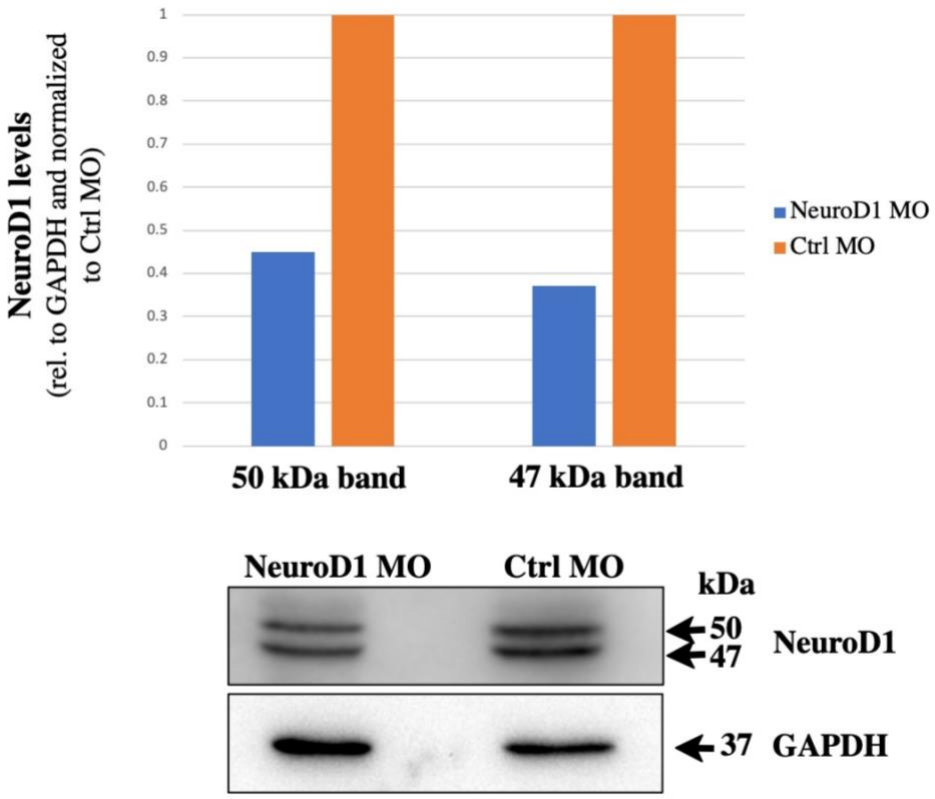

Figure 20. The NeuroD1 MO reduces NeuroD1 protein levels. At ~E1.5 (HH9^{+}-10), placode cells were unilaterally electroporated either with a NeuroD1 or control (Ctrl) MO. After re-incubation to E2.5-3 (HH16-18), the forming trigeminal ganglion on the electroporated side was dissected and pooled from multiple embryos. Lysates were prepared, and equivalent amounts of protein per sample were separated on a 14% SDS-PAGE gel. Immunoblotting for NeuroD1 and GAPDH (control) was then performed, and band intensity was calculated from unmodified immunoblot images using Image Lab software (Bio-Rad). Relative protein levels were ascertained by normalizing NeuroD1 volumes to GAPDH volumes. Knockdown amount was determined by comparing normalized ratios between Ctrl MO and NeuroD1 MO samples, with the Ctrl MO sample set as one.

4.2 NeuroD1 knockdown in trigeminal placode cells causes abnormal development of the trigeminal ganglion.

After unilateral electroporation of NeuroD1 MO using methods described in Chapter 3, the embryos were re-incubated to ~E2-2.5 (HH14-16). Then, the embryos were collected, fixed, and processed for whole-mount immunohistochemistry using an antibody to Tubb3 to detect differentiated neurons in the developing ganglia. As mentioned above, from E2.5-3.5 (HH16-21), neuronal differentiation mainly occurs in the placodal population, while starting at E4 (HH22-24), neural crest cells begin to differentiate into neurons (Hamburger, 1961; D'Amico-Martel and Noden, 1980; Shiau et al., 2008). Therefore, this antibody labels neural crest- and placode-derived neurons, depending on the developmental stage of the embryo. Confocal images of embryo heads were obtained to examine gross trigeminal ganglion morphology on the electroporated side and then compared to that on the contralateral control side (Figure 21).

At E2 (HH14) (Figure 21), changes in the trigeminal ganglion were already evident. In contrast to the contralateral control side (Figure 21A, arrowhead), the forming trigeminal ganglion is diminished in size and there appear to be fewer neurons present on the NeuroD1-depleted side (Figure 21B, arrowhead). There were also many MO-positive cells found in the electroporated ganglion (Figure 21C, F, arrows), and Tubb3-positive placodal neurons can be observed throughout the condensing ganglion. Higher magnification images (Figure 21D-F) revealed neurons that were less organized. Accordingly, neurons on the electroporated side were widely dispersed (Figure 21E), whereas those on the control side were densely packed (Figure 21D).

By E2.5 (HH16), both the electroporated and control ganglion possessed Tubb3-positive placodal neurons (Figure 22A, B, arrowheads), and MO-positive neurons were observed in the

electroporated ganglion as well (Figure 22C, F, arrows). There were, however, differences in the way the neurites, and eventual axons, developed (Figure 22A, B, arrowheads). The neurons on the contralateral control side (Figure 22D) extended axons into the eye area, whereas axons from NeuroD1 MO-electroporated neurons did not readily reach the eye (Figure 22E). Moreover, neurons within both lobes on the NeuroD1 MO-treated side exhibited an aberrant morphology (Figure 22E) compared to those on the contralateral side (Figure 22D). Additionally, neurons appear to be more dispersed on the electroporated side compared to the control (Figure 22D, E, brackets).

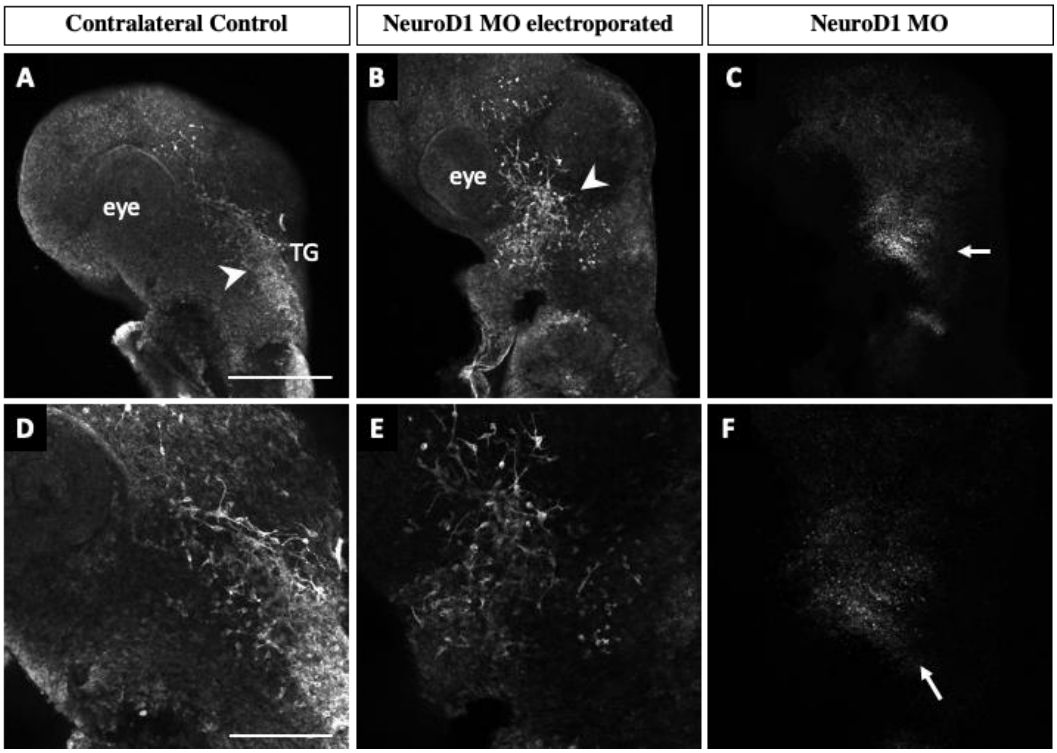

Figure 21. Depletion of NeuroD1 in trigeminal placode cells impairs trigeminal ganglion development. Lateral view of the trigeminal ganglion in a chick head (E2 (HH14), n = 3). Representative images are maximum intensity projections of confocal Z-stacks through the contralateral control (A, D) and NeuroD1 MO electroporated (B, E) side after processing for whole-mount Tubb3 immunohistochemistry to detect placode-derived neurons (A, B, D, E, arrowheads) and tissue clearing. Bottom row shows higher magnification images of the top row. (C, F) MO-positive cells (arrows). Scale bar is 500μm in (A) and applies to (B, C) and 200μm in (D) and applies to (E, F). Abbreviations: TG, trigeminal ganglion.

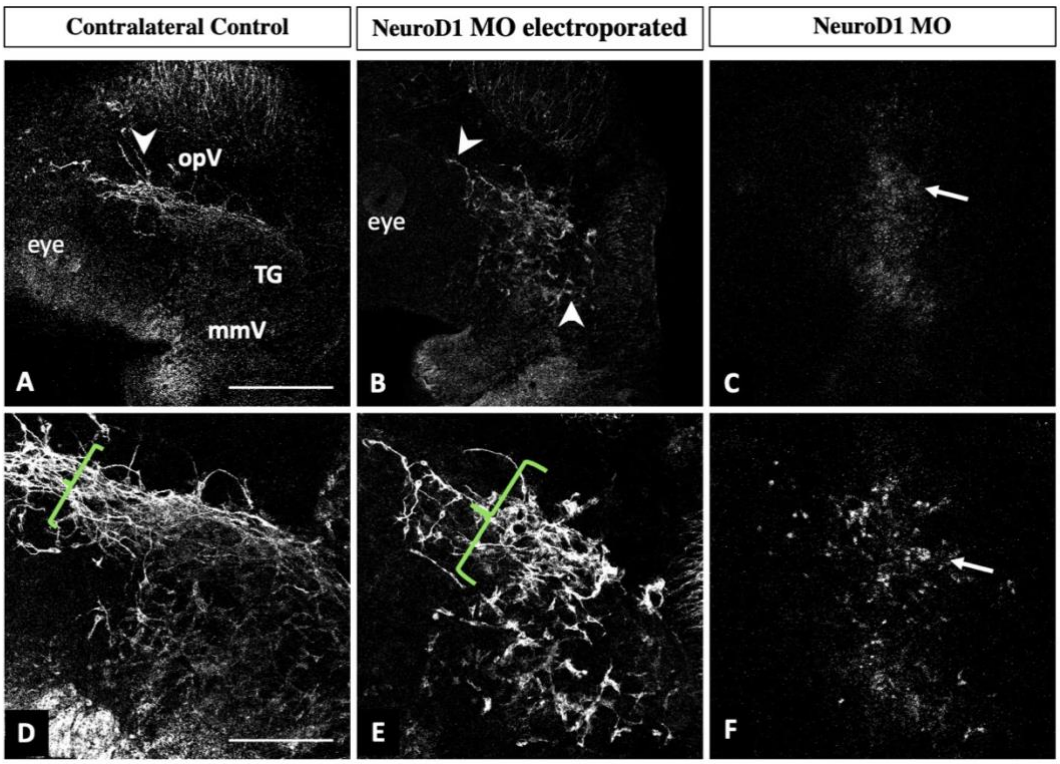

Figure 22. NeuroD1 depletion in trigeminal placode cells disrupts trigeminal ganglion development Lateral view of the trigeminal ganglion in a chick head (~E2.5 (HH16), n = 3). Representative images are maximum intensity projections of confocal Z-stacks through the contralateral control (A, D) and NeuroD1 MO electroporated (B, E) side after processing for whole-mount Tubb3 immunohistochemistry to detect placode-derived neurons (A, B, D, E, arrowheads) and tissue clearing. Bottom row shows higher magnification images of the top row. (C, F) MO-positive cells (arrows). Brackets indicate width of ophthalmic branch. Scale bar is 500μm in (A) and applies to (B, C) and 200μm in (D) and applies to (E, F) Abbreviations: mmV, maxillomandibular lobe; opV, ophthalmic lobe; TG, trigeminal ganglion.

4.3 NeuroD1 knockdown in trigeminal placode cells decreases the size of the trigeminal ganglion ophthalmic lobe.

To study the initial distribution of neurons within the trigeminal ganglion after NeuroD1 depletion, embryos were re-incubated to E2.5-3.5 (HH16-20). Successfully electroporated embryos were then sectioned and processed for immunohistochemistry using Tubb3, which, at these stages, labels placode-derived neurons.

A representative cross-section of an embryo through the forming ophthalmic lobe of the trigeminal ganglion is shown at lower magnification at E2.5 (HH16) (Figure 23A-C). Note the intensity of the Tubb3 staining varies on each side. This is likely due to this embryo being processed for whole-mount immunohistochemistry for Tubb3, followed by sectioning, and the inability of the antibody to fully penetrate the head tissue during this process. Even with this staining issue, there is little difference in ganglion morphology and size upon NeuroD1 knockdown at this axial level. As seen in higher magnification on the electroporated side, forming trigeminal neurons appeared normal (Figure 23G, arrowhead) and similar to those seen on the contralateral control side (Figure 23D, arrowhead). Many electroporated placode cells (Figure 23I) also successfully differentiated into neurons and delaminated from the ectoderm to migrate to the ganglion-forming region (Figure 23H, arrows), where they will condense with neural crest cells (not shown).

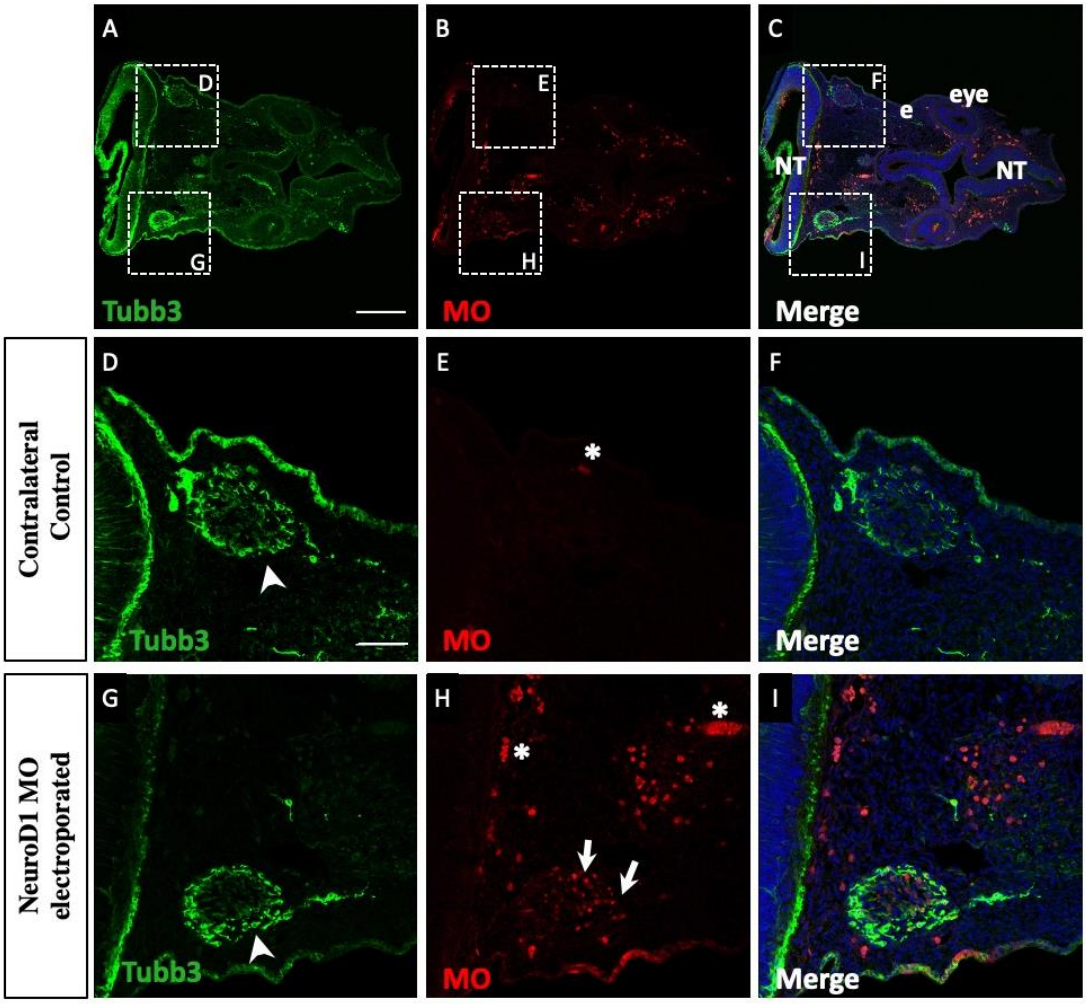

Figure 23. No qualitative difference in the size or morphology of the ophthalmic lobe of the trigeminal ganglion is observed upon knockdown of NeuroD1. Representative transverse section through the forming trigeminal ganglion (~E2.5 (HH16), n = 1) after NeuroD1 MO unilateral electroporation (B, E, H, red, short arrows) followed by Tubb3 immunohistochemistry to detect placode-derived neurons (A, C, D, F, G, I, green, arrowheads). Boxed regions in (A-C) are shown at higher magnification for the contralateral (D-F) and NeuroD1 MO-electroporated (G-I) sides. Asterisks mark red blood cells (E, H). (J) Cartoon diagram of the developing chick developing trigeminal ganglion with dashed line indicating its section plane (A to I), adapted from (Shiau and Bronner-Fraser, 2009). DAPI (blue), cell nuclei. Scale bar is 200μm in (A) and applies to (B, C) and 50μm in (D) and applies to (E-I). Abbreviations: e, ectoderm; NT, neural tube.

After only an additional 12 hours of development (E3, HH18), however, a cross-section through the ophthalmic branch revealed a smaller trigeminal ganglion after NeuroD1 knockdown compared to the contralateral control side (Figure 24A-C). Higher magnification images (Figure 24D-I) show that the ganglion possessed many MO-positive cells (Figure 24H, arrows), indicating that many of the electroporated cells delaminated and migrated from the ectoderm to coalesce with neural crest cells (not shown) and form the trigeminal ganglion. However, fewer neurons appeared to be present after NeuroD1 knockdown (Figure 24G, arrowhead) compared to the contralateral control side (Figure 24D, arrowhead).

At E3-3.5 (HH20) (Figure 25), a cross-section through the forming ophthalmic lobe of the trigeminal ganglion reveals similar phenotypes (Figure 25A-C). In contrast to what was observed on the contralateral control side of the embryo (Figure 25D, arrowhead), a reduction in NeuroD1 protein led to the formation of a smaller trigeminal ganglion (Figure 25G, arrowhead). The presence of MO-positive cells (Figure 25H, arrows) at higher magnification (Figure 25D-I) indicates that electroporated cells have delaminated from the ectoderm, migrated successfully, and are aggregating with neural crest cells (not shown) to assemble the ganglion (Figure 25G).

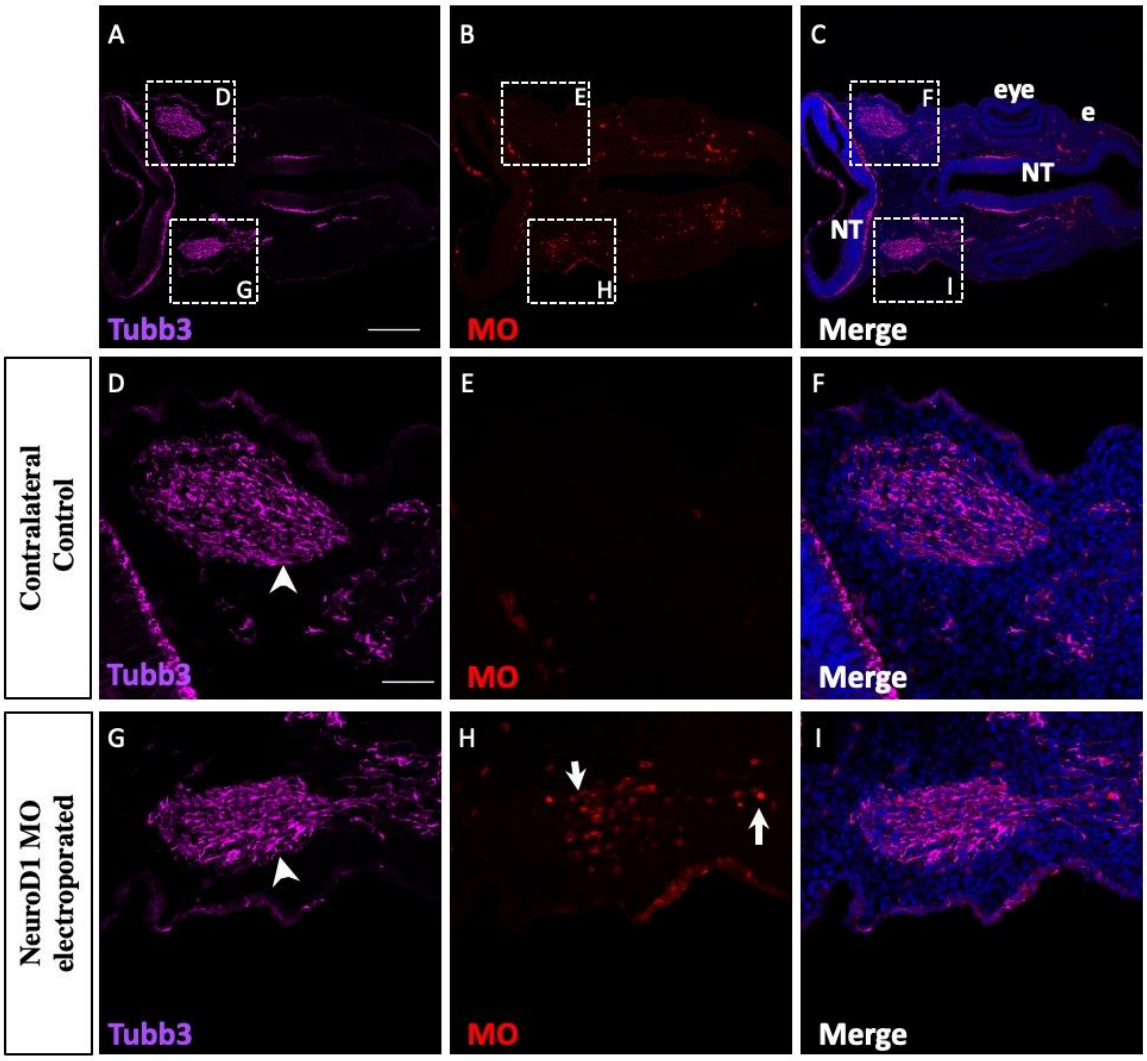

Figure 24. NeuroD1 knockdown in trigeminal placode cells decreases the size of the trigeminal ganglion ophthalmic lobe. Representative transverse section through the forming trigeminal ganglion (E3 (HH18), n = 1) after NeuroD1 MO unilateral electroporation (B, E, H, red, arrows) followed by Tubb3 immunohistochemistry to detect placode-derived neurons (A, C, D, F, G, I, purple, arrowheads). Boxed regions in (A-C) are shown at higher magnification for the contralateral (D-F) and NeuroD1 MO-electroporated (G-I) sides. (J) Cartoon diagram of the developing chick developing trigeminal ganglion with dashed line indicating its section plane (A to I), adapted from (Shiau and Bronner-Fraser, 2009). DAPI (blue), cell nuclei. Scale bar is 200μm in (A) and applies to (B, C) and 50μm in (D) and applies to (E-I). Abbreviations: e, ectoderm; NT, neural tube.

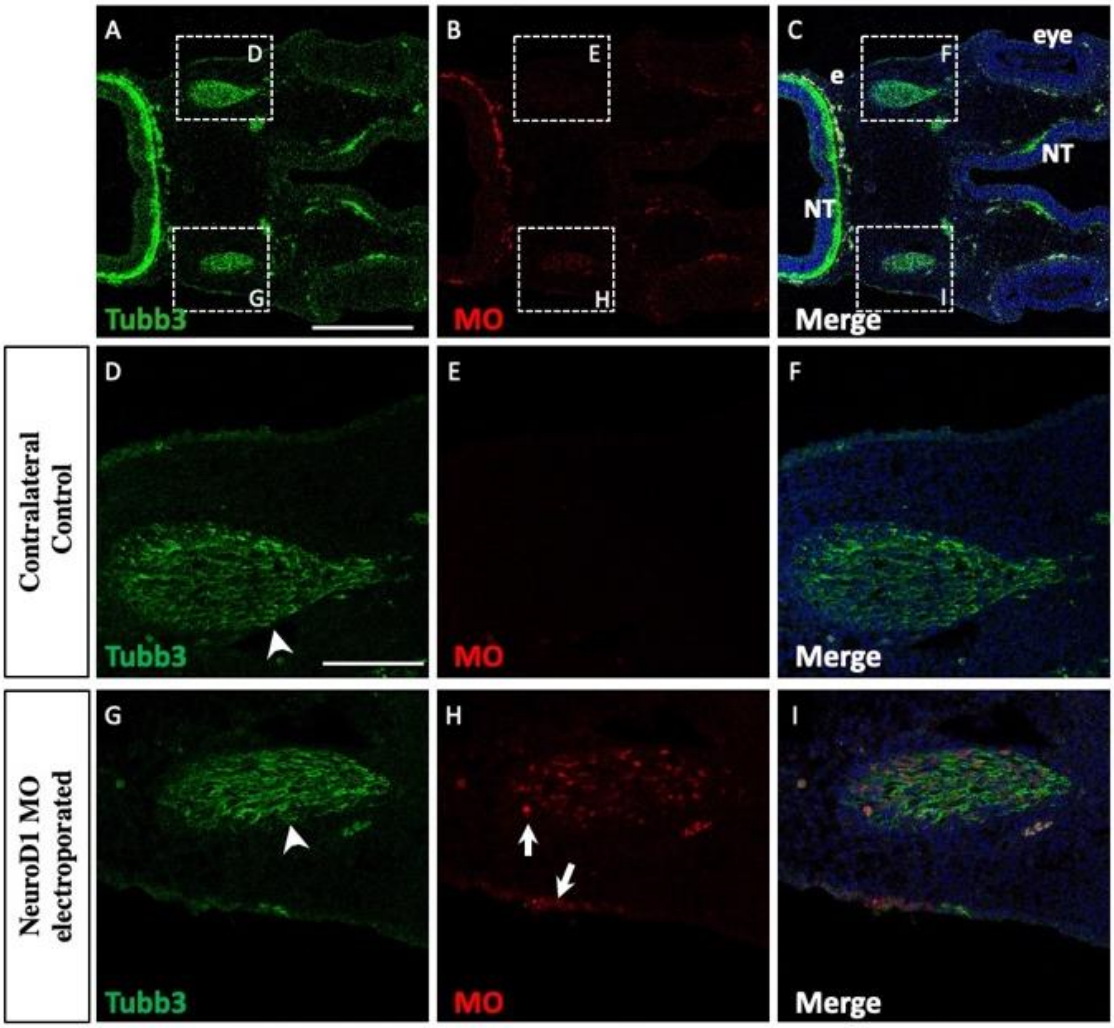

Figure 25. Trigeminal ganglion ophthalmic lobe size is decreased after NeuroD1 knockdown in placode cells. Representative transverse section through the forming trigeminal ganglion (E3-3.5 (HH20), n = 2) after NeuroD1 MO unilateral electroporation (B, E, H, red, arrows) followed by Tubb3 immunohistochemistry to detect placode-derived neurons (A, C, D, F, G, I, green, arrowheads). Boxed regions in (A-C) are shown at higher magnification for the contralateral (D-F) and NeuroD1 MO-electroporated (G-I) sides. DAPI (blue), cell nuclei. Scale bar is 200μm in (A) and applies to (B, C) and 50μm in (D) and applies to (E-I). Abbreviations: e, ectoderm; NT, neural tube.

In summary, NeuroD1 knockdown in placode cells primarily affected axons innervating the eye region, although maxillomandibular neurons also possessed an abnormal morphology (Figure 22). With older embryos, the effects of knockdown were more evident on the development of the trigeminal ganglion (Figure 22-25), leading to a reduction in ganglion size. Additionally, ophthalmic and maxillomandibular neurons appeared dispersed and less compact after NeuroD1 depletion (Figures 21, 22).

NeuroD1 protein could have multiple forms *in vivo* that are caused by post-translational modifications such as phosphorylation. Phosphorylation of Ser336 in NeuroD1 protein is essential for certain developmental processes, including dendrite growth and formation (Gaudillière et al., 2004). This modification could explain the presence of two different protein bands in the immunoblotting experiment (Figure 20). Accordingly, a 55% and 63% reduction in NeuroD1 protein impaired trigeminal gangliogenesis, providing evidence that this protein is important for trigeminal ganglion development. A higher knockdown efficiency may have more serious consequences, such as complete absence of the trigeminal ganglion or even death of the developing embryo.

In the next chapter, we investigate the expression of two cytoskeletal proteins, STMN2 and DBN1, in chick trigeminal ganglion neurons and the effects of NeuroD1 knockdown on STMN2, a target of this bHLH transcription factor in other systems (Ma et al., 1998).

Chapter 5: Evaluating the role of STMN2 and DBN1 in trigeminal ganglion growth and development

The microtubule cytoskeleton contributes to the establishment of neuronal connectivity by providing mechanical support, facilitating axonal transport, and mediating signaling events. Microtubule functions are modulated spatiotemporally by tubulin post-translational modifications and microtubule-associated proteins, which contribute to the fine-tuning of neuronal connections (reviewed by Atkins et al., 2022). Phosphorylation and dephosphorylation of STMNs, a family of four different phosphoproteins encoded by different genes and mainly expressed in the nervous system, regulate the dynamic balance of the microtubule network. These proteins also play a role in the intracellular transduction of extracellular signals (reviewed by Gagliardi et al., 2022). STMNs are involved in processes that control the differentiation of nerve cells, dendritic growth, axon formation and growth, and regulation of microtubule dynamics (Carretero-Rodriguez et al., 2021).

STMN2 regulates axon outgrowth by affecting microtubules and growth cone dynamics (Krus et al., 2022). Many of the molecular and cellular properties of STMN2 have been characterized *in vitro*, including in rat primary hippocampal cultured neurons (Morii et al., 2006), and mouse embryonic dorsal root ganglia cultures (Shin et al., 2012). Interestingly, in mouse studies, cytoskeletal regulators such as STMN2 are known to work downstream of Neurog2 and NeuroD1 (Ma et al., 1998). There is, however, limited research on the function of STMN2 *in vivo*, and specifically in chick embryos.

Neuronal migration and cytoskeletal changes are required to create functioning neurons and neuronal connections, which are induced by extra- and intracellular signaling processes (Shan et al., 2021). Despite advances in our understanding of the basic dynamics of cell

movement, it is still unclear how neurons are guided to the correct location, particularly while under the influence of extracellular cues and cytoskeletal modifications. The actin-binding protein DBN1 has been reported to be a downstream target of NeuroD1 in *Xenopus* (Seo et al., 2007). DBN1 is one of the known proteins that regulates cytoskeletal dynamics in migrating neurons (Shan et al., 2021), and it has a key role in neuronal morphogenesis (Hayashi et al., 1996). DBN1 accumulates in the somata of migrating neurons and in the neurites of postmigratory neurons during embryonic development (Hayashi et al., 1996). DBN1 both binds to, and bundles, actin filaments. When DBN1 is bound to actin filaments, the microtubule-binding protein EB3 binds DBN1, allowing for the coupling of microtubules and actin filaments in the growth cone of neuronal cells. Coordination of actin filaments and microtubules in the growth cone is necessary to respond appropriately to growth cone guidance cues (Gordon-Weeks, 2016).

Given that STMN2 and DBN1 are Neurog2 and NeuroD1 targets in other systems, the third goal of this study was to determine whether STMN2 and DBN1 are expressed in the trigeminal ganglion of chick embryos, as well as to investigate the role of NeuroD1 in regulating STMN2.

5.1 STMN2 protein is present in the chick embryonic trigeminal ganglion.

To determine whether STMN2 is expressed in the trigeminal ganglion, immunohistochemistry for STMN2 and Tubb3, which labels placode-derived neurons at this developmental stage, was performed on sections taken through this region in wildtype chick embryos at E3-3.5 (HH20). STMN2 expression was observed in the trigeminal ganglion (Figure

26B, C, E, F), specifically in all Tubb3-positive placode-derived neurons (Figure 26F, arrows). STMN2 was also detected in the ectoderm (Figure 26E, caret).

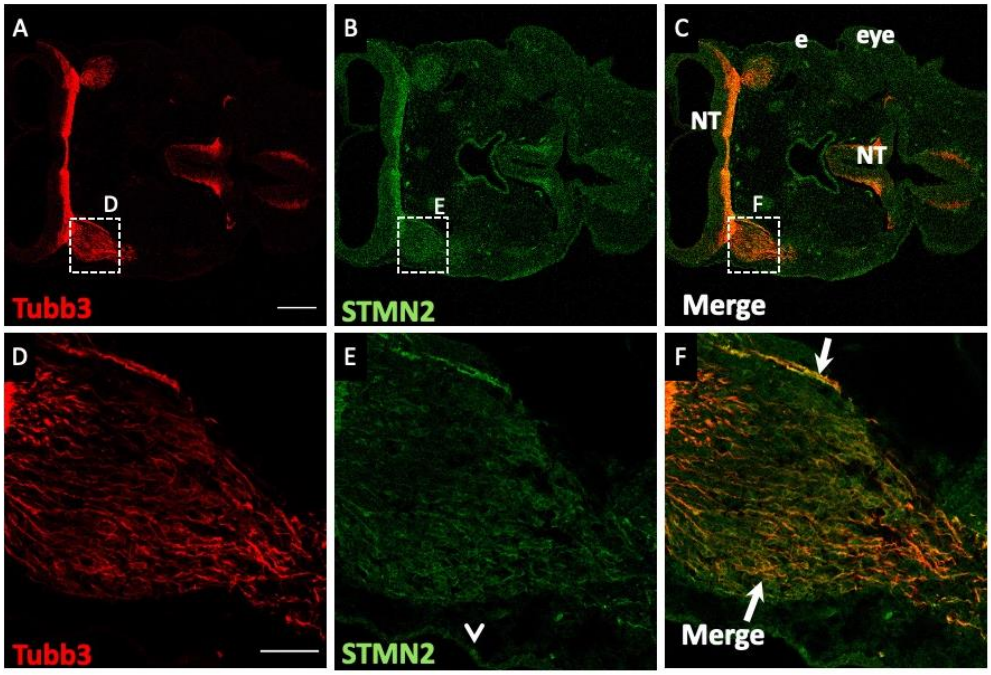

Figure 26. STMN2 expression is detected in the trigeminal ganglion of the chick embryo. Representative transverse section through the forming trigeminal ganglion (E3-3.5 (HH20), n = 1) in wildtype chick embryos after immunohistochemistry for STMN2 (B, C, E, F, green) and Tubb3 (A, C, D, F, red). Arrows point to Tubb3-positive neurons that are STMN2-positive, while the caret marks STMN2-positive ectoderm. Scale bar is 200μm in (A) and applies to (B, C) and 50μm in (D) and applies to (E, F). Abbreviations: e, ectoderm; NT, neural tube.

5.2 Knockdown of NeuroD1 in trigeminal placode cells does not impact STMN2 expression in the trigeminal ganglion.

We sought to determine effects on STMN2 expression and distribution within the trigeminal ganglion after NeuroD1 depletion. Using the methods described in prior chapters, we unilaterally electroporated trigeminal placode cells with NeuroD1 MO, and then re-incubated embryos to E3-3.5 (HH20). Successfully electroporated embryos were processed for sectioning, followed by immunohistochemistry using antibodies to STMN2 and Tubb3, which, at this stage, labels placode-derived neurons. Examination of serial transverse sections through the developing ophthalmic lobe of the trigeminal ganglion uncovered many MO-positive cells within the electroporated ganglion (Figure 27C, K, arrow). These sections also revealed a smaller trigeminal ganglion after NeuroD1 depletion (Figure 27A), which was confirmed at higher magnification (Figure 27I). However, no change was noted in STMN2 expression or distribution after NeuroD1 knockdown (Figure 27J, arrowheads). Due to the smaller trigeminal ganglion observed on the electroporated side, there were fewer STMN2- and Tubb3-double-positive cells in the trigeminal ganglion after NeuroD1 depletion (Figure 27J, arrowheads) when compared to the contralateral control side (Figure 27F, arrowheads).

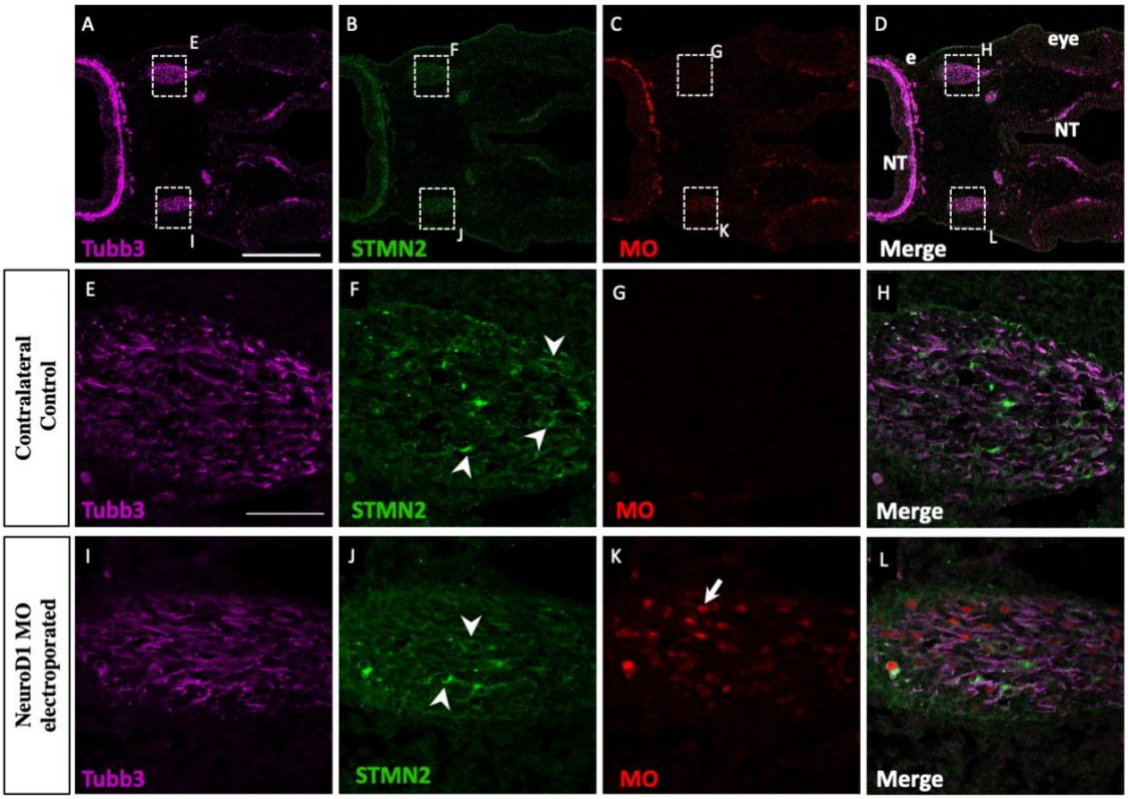

Figure 27. STMN2 expression is unaffected in the ophthalmic lobe of the trigeminal ganglion after NeuroD1 knockdown in trigeminal placode cells. Representative transverse section through the forming trigeminal ganglion (E3-3.5 (HH20), n = 2) after NeuroD1 MO unilateral electroporation (C, G, H, red, arrow) followed by Tubb3 immunohistochemistry to detect placode-derived neurons (A, D, E, H, I, L, purple) and STMN2 (B, D, F, H, J, L, green, arrowheads). Boxed regions in (A-D) are shown at higher magnification for the contralateral (E-H) and NeuroD1 MO-electroporated (I-L) sides. Scale bar is 200μm in (A) and applies to (B-D) and 50μm in (E) and applies to (F-L). Abbreviations: e, ectoderm; NT, neural tube.

5.3 DBN1 protein is present in cultured chick embryonic trigeminal neurons.

For the purpose of determining DBN1 expression in the trigeminal ganglion, immunocytochemistry for DBN1 and Tubb3 was performed on explant cultures of wildtype chick trigeminal ganglion neurons. The trigeminal ganglion-forming region (ectoderm containing trigeminal placode cells, migratory neural crest cells, and some cranial mesenchyme), was dissected at ~E2 (HH14) and cultured *ex vivo* for 48 hours. In these cultures, DBN1 expression (Figure 28B, arrow) was observed in Tubb3-positive trigeminal neurons (Figure 28A).

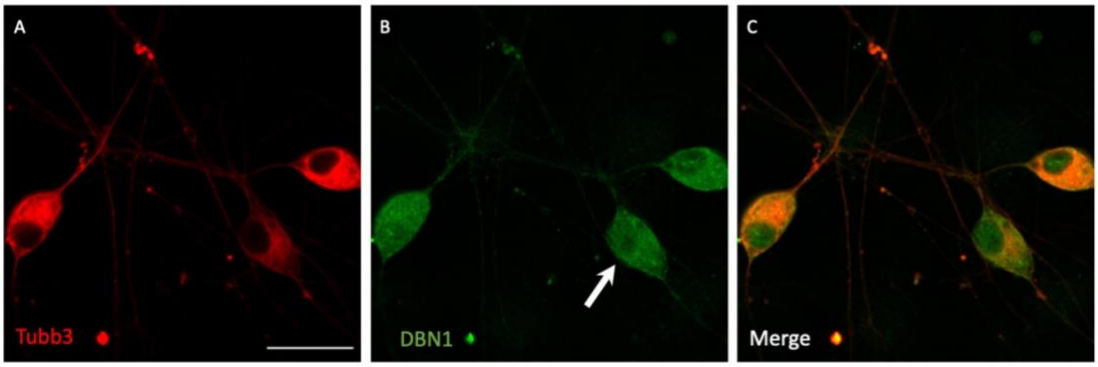

Figure 28. DBN1 expression is detected in cultured chick trigeminal ganglion neurons. Representative culture of trigeminal ganglion neurons (n = 2) from wildtype chick embryos after immunohistochemistry for Tubb3 (A, C, red) and DBN1 (B, C, green, arrow). Scale bar is 25μm in (A) and applies to all images.

In summary, STMN2 was observed in trigeminal ganglion placode-derived neurons and in the ectoderm (Figure 26). Knockdown of NeuroD1 did not appear to affect the expression of STMN2 in neurons residing in the ophthalmic branch of trigeminal ganglion at the examined stage (E3-3.5). These results suggest that STMN2 may not be regulated by NeuroD1, at least not at this developmental stage. DBN1 was also found to be expressed in cultured chick trigeminal ganglion neurons (Figure 28). This culture method was chosen because the DBN1 antibody failed to work on whole embryos or sections, making it difficult to also evaluate the effects of NeuroD1 knockdown on DBN1 in the context of the forming trigeminal ganglion *in vivo*.

Chapter 6: Discussion

6.1 Introduction

Neural crest and cranial placodes play a crucial role in embryonic development. These cells give rise to many different cell types in vertebrates, including bone, cartilage, and pigment cells, and sensory neurons and glia of the peripheral nervous system (reviewed by Bronner and LeDouarin, 2012). Interactions between neural crest cells and ectodermal placodes are required to form the cranial trigeminal ganglion, which is involved in the perception of touch, pressure, temperature, and pain in the head and face (reviewed by Koontz et al., 2022). Because of the various cell types into which neural crest cells can differentiate, many disorders can result from neural crest cell dysfunction. These are termed neurocristopathies and include structural malformations such as cleft lip and palate (review by Trainor, 2010) as well as neuroblastoma, the most commonly occurring extracranial malignant tumor in children (Nagashimada et al., 2012). Moreover, defects in placode cells have been linked to neurodevelopmental disorders such as blindness (Bhattacharyya et al., 2004), deafness (Maharana et al., 2021), and loss or diminished sense of smell (Bricker et al., 2022). Altogether, a better understanding of neural crest and placode cell ontogeny is critical to treat and/or prevent conditions arising from deficiencies in neural crest and placode cell development.

In our research, we have used the developing chicken embryo to study trigeminal ganglion development. Chicken embryos make excellent models, as chickens and mammals share some morphological, biochemical, and genetic similarities (Brugmann et al., 2010). Therefore, the genes involved in controlling trigeminal ganglion development in birds are also likely conserved during these same processes in mammals. Identification of these genes may aid in understanding the pathogenesis of craniofacial abnormalities in animals and humans

(Brugmann et al., 2010). Therefore, it is critical to determine how gene regulatory networks control craniofacial development and neurogenesis.

6.2 The importance of the bHLH transcription factors Neurog2 and NeuroD1 in trigeminal gangliogenesis

Neurogs belong to the bHLH transcription factor family and are known to play a crucial role in the development of placode-derived cranial sensory neurons. In the chick embryo, Neurog2 is expressed primarily in ophthalmic trigeminal placodes, and it is required to form trigeminal sensory neurons. Other transcription factors may facilitate the development of placode-derived sensory neurons by acting downstream of Neurogs (Begbie et al., 2002). *NeuroD1* has been suggested to be a target of Neurogs as revealed by *in situ* hybridization studies in mouse (Ma et al., 1998), but this has not been rigorously examined.

Additionally, there is a close temporal connection between neurogenesis and cell migration, but the molecular link between them is unknown. Ge et al. (2006) proposed that regulation of actin and microtubules is essential for successful neuronal migration. Intriguingly, studies performed in *Xenopus* demonstrated that Neurogs and NeuroD1 transcriptionally regulate genes whose protein products function in controlling cell morphology and migration (Seo et al., 2007). Among the downstream targets of Neurogs and NeuroD1 that regulate cell polarity and the cytoskeleton are *STMN2* (Ma et al., 1998) and *DBN1* (Seo et al., 2007). Besides their known expression pattern in the chick embryo, the function of Neurog2 and NeuroD1 during trigeminal gangliogenesis is still poorly understood. The goal of this study was to determine the function of Neurog2 and NeuroD1 in trigeminal ganglion development, and in the context of the regulation of *STMN2* and *DBN1*.

To address Neurog2 and NeuroD1 function, knockdown experiments were performed using MOs, which have advantages and disadvantages for studying gene function. The non-ionic backbone of the MO reduces interactions with proteins, thereby eliminating potential non-specific mechanisms of action (Ferguson et al., 2014; Moulton, 2017; Nan and Zhang, 2018). Further, MOs bind their complementary RNA sequences with greater affinity than DNA binds RNA (Ferguson et al., 2014; Moulton, 2017; Nan and Zhang, 2018). MO-mediated knockdown *in vivo* is relatively long-term, as MOs can persist in embryos (and cultured cells) up to a week or more after delivery and are also fairly stable and resistant to nucleases (Nan and Zhang, 2018). Disadvantages associated with MOs include their ability to become diluted, and thus less active, with the growth and division of cells. Moreover, high transcription rates can inhibit their function (Nan and Zhang, 2018). Because these advantages outweigh the disadvantages, MOs have been extensively used as tools to study gene function during embryonic development.

As an established model system for developmental biology research, the chick embryo is well suited to performing loss-of-function studies by electroporating MOs into specific cell types (Mende et al., 2008). By using MOs, we were able to knockdown Neurog2 and NeuroD1 in a spatially and temporally controlled manner, targeting trigeminal placode cells in the ectoderm. Cell population and embryo age are important factors that determine whether MOs will be successful in knockdown experiments. Generally, MOs do not work well in rapidly dividing cells due to the effect of MO dilution. Using MOs is appropriate for our study, however, since we are targeting a cell population (placode cells) that stops dividing fairly quickly due to its differentiation shortly after MO introduction.

Electroporation of Neurog2 MO into trigeminal placode cells led to a partial reduction in Neurog2 protein levels, but the observed phenotype suggests that the protein plays an important

role during trigeminal gangliogenesis. Given the results noted in mouse *Neurog2* knockout experiments (Ma et al., 1998), severe consequences may result if 100% knockdown efficiency is achieved, such as complete loss of the trigeminal ganglion, serious craniofacial anomalies, or even embryonic death.

Upon electroporation with NeuroD1 and control MOs, immunoblotting for NeuroD1 protein revealed two distinct bands. Based on the fact that both bands showed a reduction after knockdown, we speculate that both represent NeuroD1 protein. The presence of two bands could be caused by post-translational modifications such as phosphorylation of NeuroD1, leading to this shift in electrophoretic mobility. We could test this hypothesis by treating lysates with a phosphatase, thereby removing any phosphate groups from the protein, and allowing potentially one band to appear after immunoblotting if phosphorylation caused the shift in band mobility.

As a result of Neurog2 and NeuroD1 knockdown, the development of the trigeminal ganglion was negatively impacted, with a decrease in size of the trigeminal ganglion and associated nerve structures (Figure 12-17, 21-25). A reduction in trigeminal ganglion size could be due to, among other things, delayed delamination of placode cells contributing to the ganglion, increased cell death, or both. MO-positive cells are abundant in the ganglion, indicating that many electroporated cells have delaminated and migrated from the ectoderm. Thus, we can speculate that Neurog2 and NeuroD1 knockdown did not completely prevent placode cell delamination and migration. To determine if Neurog2 or NeuroD1 depletion delays delamination, we could perform live imaging of fluorescently-labeled placode cells as they develop. A combination of plasmids expressing histone H2B-RFP, along with a cytoplasmic or membrane GFP reporter, would be optimal for labeling and imaging placode cells, as cytoplasmic/membrane markers determine cell shape, while nuclear markers allow for the

identification of individual cells (Shiau et al., 2011). Due to the red fluorescent nature of our designed MO, we could use a protein that fluoresces differently than RFP to mark the chromatin, and a GFP reporter for the cytoplasm/membrane. Placode delamination would then be visualized by recording Z-stack, time-lapse images in cranial slice cultures electroporated with Neurog2 or NeuroD1 MO and comparing those with controls, as in (Shiau et al., 2011).

Future studies could also quantify various aspects of trigeminal ganglion neurodevelopment after Neurog2 or NeuroD1 knockdown in whole embryos and sections through the forming trigeminal ganglion. Whole embryo heads stained with Tubb3 (older than E3 ($\geq$HH18)) would be subjected to FRUIT clearing, followed by collection of Z-stack images using confocal microscopy. After collection of Z-stacks, the entire area of the trigeminal ganglion and its nerves could be measured using the ImageJ area calculation function. Next, the innervation field of the trigeminal ganglion and its branches could be quantified. The nerves would be traced using the Simple Neurite Tracer plug-in in ImageJ, and nerve branching complexity quantified using the Sholl Analysis function within ImageJ. Additionally, to evaluate changes in cell morphology, section immunohistochemistry could be performed using neural crest and placode cell markers and confocal microscopy. To observe the impact of Neurog2 or NeuroD1 knockdown on the development of neurons in a single layer, trigeminal ganglion explant cultures could be prepared and processed for immunocytochemistry using neuronal markers such as Tubb3.

Proper trigeminal ganglion formation relies on regulated and reciprocal interactions between placode cells and neural crest cells (Shiau et al., 2008). Although we hypothesize that Neurog2 or NeuroD1 knockdown will not have a non-cell autonomous effect on neural crest cells, this line of investigation should still be pursued to rule out any potential effects on this cell

population. With appropriate antibodies to label early neural crest cells (e.g., HNK-1) and their glial derivatives (e.g., Sox10, Cad7), it is possible to examine the impact of Neurog2 or NeuroD1 knockdown on neural crest cells through immunohistochemistry. To compare against controls, neural crest cells and their derivatives should be counted using the above-mentioned markers. If we observe changes in neural crest cells and their derivatives, this would mean that knockdown of Neurog2 or NeuroD1 in placode cells has a non-cell autonomous effect on neural crest cells.

Interestingly, at later stages of development after Neurog2 knockdown, some MO-negative neurons appeared less condensed (Figure 17). These could be placodal neurons that were not electroporated or instead are neurons derived from the neural crest. Neurog2 depletion may therefore decrease the size of the trigeminal ganglion by influencing the assembly of neurons within it or by having a non-cell autonomous effect on neural crest cells, as discussed above. At stages HH3.5-4.5 (HH22-24), Tubb3 marks both neurons derived from neural crest and placode cells. To test the hypothesis of a non-cell autonomous effect on specifically neural crest cell-derived neurons, it is first necessary to differentiate neural crest from placodal neurons. One approach to do this is to electroporate a GFP expression construct into the dorsal neural tube where the neural crest cells reside, or in the ectoderm prior to placode delamination, in order to visualize the specific cell population later on in development.

Use of TUNEL staining or phospho-histone H3 immunohistochemistry would demonstrate whether the reduction in trigeminal ganglion size after Neurog2 or NeuroD1 knockdown is due to alterations in cell death or proliferation, respectively. These methods would be carried out on sections taken through the forming trigeminal ganglion to identify apoptotic or actively proliferating cells, together with markers for neural crest cells (e.g., Sox10) and placodal neurons (e.g., Islet-1). These nuclear markers would facilitate cell counting to assess the impact

on these two cell populations in the trigeminal ganglion with respect to whether they are dividing or dying. Depending on the developmental stage, it may be possible to note some neural crest cell proliferation; however, if these cells have already divided and differentiated into neurons starting at E4 (HH22-24), proliferation is unlikely to be detected. Under normal conditions, placodal neurons will have already differentiated, so there should be little to no proliferation observed in them.

Given this and our finding that the trigeminal ganglion on the Neurog2 MO- and NeuroD1 MO-electroporated sides are smaller, we speculate that placodal neuron death may be increased during the formation and development of the trigeminal ganglion after Neurog2 and NeuroD1 knockdown. Moreover, we predict that neither Neurog2 nor NeuroD1 knockdown will affect neural crest cells. However, further investigation at different developmental stages is needed to clarify this. In the absence of any differences in cell number, we would investigate whether abnormal trigeminal ganglion development is due to changes in neuron organization caused by alterations in cytoskeletal protein regulation, expression, and localization (see below).

Growth of axons is regulated by guidance molecules, adhesion proteins, and neurotrophic factors (Deinhardt et al., 2011). A functional nervous system depends on an orderly network of connections between neurons. In establishing this neural network, there are both progressive and regressive elements involving neurogenesis and axonal outgrowth, and neuronal death and axon retraction, respectively (He et al., 2002). To prevent inappropriate axonal projections, neuronal death or selective retraction occurs extensively. There are different types of physiological cues that induce axonal retraction, including changes in the cytoskeleton (He et al., 2002).

Interestingly, we observed improper innervation of the eye area after Neurog2 and NeuroD1 knockdown (Figures 12-14, 21, 22). In light of these findings and the need for

progressive and regressive events during nervous system development as discussed above, Neurog2 and/or NeuroD1 may regulate downstream targets that affect these processes. This could include controlling the expression of neurotrophin receptors (e.g., Tropomyosin receptor kinase (Trk) family of receptors), as lack of neurotrophic support leads to target innervation defects, which ultimately result in neuronal cell death (Barde, 1994; Liebl et al., 1997), or even modulating expression of neurotrophic factors themselves. Studies have shown that the neurotrophic factor nerve growth factor (NGF), which binds to TrkA, is required for the survival of most mature neurons in the peripheral nervous system (Parada et al., 1992; Liebl et al., 1997). Brain-derived neurotrophic factor (BDNF) and neurotrophin-3 (NT-3) are other neurotrophic factors that are essential for the survival and maintenance of trigeminal neurons (Hallbook et al., 2003, Ji and Jaffrey, 2012). Future studies should be geared at addressing the impact of Neurog2 and NeuroD1 knockdown on the expression of Trk receptors and/or their ligands. We speculate that blocking Trk receptors or their ligands, either pharmacologically or molecularly, might have the same effect as inhibiting Neurog2 or NeuroD1 if either transcription factor controls Trk receptor or neurotrophic factor expression.

Alternatively, it is possible that ophthalmic neurons reached their target tissues normally after Neurog2 or NeuroD1 depletion, but then retracted due to compromised cytoskeletal modifications caused by Neurog2 and/or NeuroD1 knockdown. Previous studies in mice (Ma et al., 1998) and *Xenopus* (Seo et al., 2007) demonstrated that cytoskeletal regulators are downstream targets of bHLH transcription factors. Live imaging could be used to test this hypothesis by measuring the changes in axon length over time after Neurog2 or NeuroD1 knockdown. The role of Neurog2 and NeuroD1 in controlling expression of potential cytoskeletal regulators in this context is discussed in more detail below.

Neurog2 knockdown also impaired the separation of the maxillomandibular branch into definitive maxillary and mandibular branches at E3 (HH18) (Figure 12). At older stages, E3-3.5 (HH20), maxillary neurons appeared more dispersed but were still arranged in bundles (Figure 13). These data suggest Neurog2 may regulate nerve branching and separation into the maxillary and mandibular nerves. Aberrant neuronal development could indicate that knockdown affects the maturation and morphology of neurons.

The similarity in phenotypes obtained after Neurog2 and NeuroD1 knockdown begs the question as to whether these proteins function in a common pathway as suggested in previous studies performed in mouse (Ma et al., 1998) and *Xenopus* (Seo et al., 2007). Future experiments could include using quantitative PCR (qPCR) to determine if *NeuroD1* is a transcriptional target of Neurog2 by monitoring changes in *NeuroD1* transcript levels after Neurog2 depletion. We hypothesize that *NeuroD1* transcript levels will decrease after Neurog2 knockdown. To confirm that the phenotypes observed after Neurog2 knockdown are due primarily to a reduction/loss of *NeuroD1* expression, we could co-electroporate a *NeuroD1* expression construct after Neurog2 knockdown, which should at least partially rescue the Neurog2 knockdown phenotype. If the *NeuroD1* expression construct does not rescue the Neurog2 knockdown phenotype, this would provide evidence that these two transcription factors reside in different pathways.

Since Neurog2 functions in the multipolar-to-bipolar transition of placode-derived neurons (Heng et al., 2008), one potential phenotype after Neurog2 knockdown would be an increase in neurons with a multipolar morphology in the electroporated embryos compared to the controls, which could eventually lead to improper trigeminal ganglion development. The bipolar morphology of mature neurons is characterized by two processes at opposite ends of the cell body. In contrast to mature placodal neurons, newly delaminated placodal cells have two or more

short axonal processes (Shiau et al., 2011). An assessment of neuronal processes could be conducted on sections of the developing trigeminal ganglion and/or in trigeminal neurons in explant cultures. As a result, we would be able to examine the impact of knockdown on the maturation of neurons from multipolar to mature bipolar types.

As noted previously, knockdown of Neurog2 and NeuroD1 could negatively affect the innervation of target tissues by disrupting the formation of neuronal processes and nerves. For example, Neurog2 and NeuroD1 may play an essential role in regulating membrane dynamics and cytoskeletal rearrangements that are required for the formation of these axonal processes. If fewer neurons are observed in the trigeminal ganglion after Neurog2 or NeuroD1 knockdown, but neuron branching and morphology appear to be normal, this would indicate that the neurons that managed to delaminate toward the trigeminal ganglion are able to mature and form bipolar neurons. Having fewer neurons in the trigeminal ganglion could also mean that the absence of Neurog2 and NeuroD1 impacts neurogenesis and the delamination and migration of neurons. Aberrant neuronal development would indicate that knockdown affects the maturation and morphology of neurons. It is important to note that these ideas are not mutually exclusive such that Neurog2 and/or NeuroD1 could be affecting both neurogenesis/delamination and neuronal maturation.

Our current study depleted Neurog2 and NeuroD1 early in placode cell development by introducing MOs after placode cell specification but prior to delamination. To determine the role of Neurog2 and NeuroD1 later in development (i.e., after delamination), it may be possible to knockdown these transcription factors using inducible shRNA constructs. We could observe the development of the trigeminal ganglion using whole-mount, section, or explant immunohistochemistry after these knockdown experiments.

6.3 The role of Neurog2 and NeuroD1 in modulating the neuronal cytoskeleton

After Neurog2 or NeuroD1 knockdown, it would be worthwhile to examine the cytoskeletal regulators STMN2 and DBN1 to determine whether the observed defects are related to their dysfunction. In transverse sections taken through the ophthalmic lobe of the trigeminal ganglion, we detected expression of STMN2. In chick embryos, however, no published data are available regarding DBN1 expression in the trigeminal ganglion. By performing immunohistochemistry on explanted trigeminal ganglia tissue, we demonstrated that DBN1 is expressed in trigeminal neurons. The next step would be to perform immunocytochemistry on whole embryos and sections at different stages to determine when DBN1 protein is first detected, contingent upon the availability of a working antibody.

To determine if trigeminal ganglion phenotypes observed after Neurog2 or NeuroD1 knockdown are caused by changes in *DBN1* and *STMN2*, qPCR could be used to measure their transcripts levels after Neurog2 or NeuroD1 depletion. No change in *DBN1* and *STMN2* transcript levels by qPCR would likely indicate that Neurog2 and NeuroD1 do not transcriptionally regulate these genes. If alterations in transcript levels are observed, we also predict we may observe changes in the localization and/or levels of DBN1 and STMN2 proteins by immunohistochemistry or immunoblotting. If no changes are observed in the localization or levels of DBN1 and STMN2 after knockdown of Neurog2 or NeuroD1, this would also suggest that these gene products are not controlled by Neurog2 or NeuroD1.

If DBN1 and STMN2 are in the same pathway as Neurog2 and/or NeuroD1, then depletion of DBN1 or STMN2 might lead to phenotypes similar to that observed after Neurog2 or NeuroD1 knockdown. We also may be able to establish a “wildtype” phenotype after Neurog2 or NeuroD1 knockdown by co-electroporation of a *DBN1* and/or *STMN2* expression construct. If

Neurog2 and/or NeuroD1 knockdown phenotypes are not recapitulated after DBN1 and/or STMN2 knockdown, it is possible that other proteins with similar roles might compensate for the lack of DBN1 and STMN2, and/or further indicate that these bHLH transcription factors do not regulate DBN1 and STMN2. It is important to note, however, that depleting upstream transcription factors like Neurog2 or NeuroD1 is more likely to have a severe effect since these transcription factors control many other genes that may ultimately cause the observed trigeminal ganglion defects.

To address a potential impact on other genes, both targeted and global approaches can be taken in the chick model. Among candidate proteins and pathways that could be affected by Neurog2 and/or NeuroD1 are neurotrophic signaling pathways involving NGF, BDNF, and NT-3, as well as TrkA, TrkB, and TrkC receptors; Neurog1 and other bHLH transcription factors such as NeuroD4 and NHLH1 (see Figure 8); and other proteins that regulate the cytoskeleton and cell polarity. One way to identify other genes controlled by Neurog2 or NeuroD1 is to perform qPCR and assess the transcript levels of downstream targets identified in other animal models (Ma et al., 1998; Seo et al., 2007). It may be possible to discover novel downstream targets of Neurog2 and NeuroD1 by overexpressing or knocking down these transcription factors in placode cells, performing RNA-seq on developing chick trigeminal ganglion tissue, and identifying changes in gene expression. RNA-seq results could then be validated through a variety of ways. First, candidate targets should be expressed in relevant cell types within the trigeminal ganglion, and this could be evaluated by performing *in situ* hybridization, immunohistochemistry, and/or immunoblotting (if appropriate antibodies are available). Next, we could perform qPCR for candidate transcripts in trigeminal ganglion tissue after knockdown of Neurog2 or NeuroD1 to confirm RNA-seq results. Finally, immunohistochemistry on sections

taken through the forming trigeminal ganglion at different stages after knockdown may reveal changes in the protein product of the affected transcript.

6.4 Summary

Errors in craniofacial development can have a significant impact on animal and human welfare and result in embryo loss or the birth of viable offspring with craniofacial anomalies. Breeders may also suffer economic losses due to animal death caused by congenital malformations arising from defects in neural crest or placode cells. Craniofacial disorders are a primary cause of infant mortality, and they have serious ramifications for children and parents in terms of functional, aesthetic, and social aspects (reviewed by Trainor, 2010). Developing treatment strategies for diseases and defects associated with neural crest- and placode-derived sensory organs requires an understanding of how signaling pathways and transcription factors function during development (reviewed by Singh and Groves, 2016). In order to shed new light on this regulatory network, we focused our study on Neurog2 and NeuroD1, which are critical to neurogenesis and the successful development of the trigeminal ganglion. Through knockdown experiments, we demonstrated that Neurog2 and NeuroD1 function in proper trigeminal ganglion formation and neurogenesis. Further, depletion of these transcription factors indicated that they are necessary for proper axon growth and innervation of target tissues. Studies such as these will not only contribute to our understanding of trigeminal ganglion development but will also expand our knowledge of diseases of the peripheral nervous system in animals and humans.

References

Abu-Elmagd, Muhammad, et al. "cSox3 expression and neurogenesis in the epibranchial placodes." *Developmental biology* 237.2 (2001): 258-269.

Atkins, Melody, Xavier Nicol, and Coralie Fassier. "Microtubule remodelling as a driving force of axon guidance and pruning." *Seminars in Cell & Developmental Biology*. Academic Press, 2022.

Baker, Clare VH, and Marianne Bronner-Fraser. "Vertebrate cranial placodes I. Embryonic induction." *Developmental biology* 232.1 (2001): 1-61.

Barde, Yves Alain. "Neurotrophins: a family of proteins supporting the survival of neurons." *Progress in clinical and biological research* 390 (1994): 45-56.

Basch, Martín L., Marianne Bronner-Fraser, and Martín I. García-Castro. "Specification of the neural crest occurs during gastrulation and requires Pax7." *Nature* 441.7090 (2006): 218-222.

Begbie, Jo, and Anthony Graham. "Integration between the epibranchial placodes and the hindbrain." *Science* 294.5542 (2001): 595-598.

Begbie, Jo, Marc Ballivet, and Anthony Graham. "Early steps in the production of sensory neurons by the neurogenic placodes." *Molecular and Cellular Neuroscience* 21.3 (2002): 502-511.

Bhattacharyya, Sujata, et al. "Segregation of lens and olfactory precursors from a common territory: cell sorting and reciprocity of Dlx5 and Pax6 expression." *Developmental biology* 271.2 (2004): 403-414.

Bricker, Rebecca L., et al. "A molecular analysis of neural olfactory placode differentiation in human pluripotent stem cells." *Stem Cells and Development* ja (2022).

Bronner, Marianne E., and Nicole M. LeDouarin. "Development and evolution of the neural crest: an overview." *Developmental biology* 366.1 (2012): 2-9.

Bronner, Marianne E., and Marcos Simões-Costa. "The neural crest migrating into the twenty-first century." *Current topics in developmental biology* 116 (2016): 115-134.

Brugmann, Samantha A., and Sally A. Moody. "Induction and specification of the vertebrate ectodermal placodes: precursors of the cranial sensory organs." *Biology of the Cell* 97.5 (2005): 303-319.

Brugmann, S. A., et al. "Comparative gene expression analysis of avian embryonic facial structures reveals new candidates for human craniofacial disorders." *Human molecular genetics* 19.5 (2010): 920-930.

Busskamp, Volker, et al. "Rapid neurogenesis through transcriptional activation in human stem cells." *Molecular systems biology* 10.11 (2014): 760.

Carretero-Rodriguez, Luis, et al. "The Rac-GAP alpha2-chimaerin signals via CRMP2 and stathmins in the development of the ocular motor system." *Journal of Neuroscience* 41.31 (2021): 6652-6672.

Corey, David R., and John M. Abrams. "Morpholino antisense oligonucleotides: tools for investigating vertebrate development." *Genome biology* 2.5 (2001): 1-3.

Crane, Jennifer F., and Paul A. Trainor. "Neural crest stem and progenitor cells." *Annu. Rev. Cell Dev. Biol.* 22 (2006): 267-286.

D'Amico-Martel, Adele, and Drew M. Noden. "An autoradiographic analysis of the development of the chick trigeminal ganglion." (1980): 167-182.

Deinhardt, Katrin, et al. "Neuronal growth cone retraction relies on proneurotrophin receptor signaling through Rac." *Science signaling* 4.202 (2011): ra82-ra82.

Dent, Erik W., Stephanie L. Gupton, and Frank B. Gertler. "The growth cone cytoskeleton in axon outgrowth and guidance." *Cold Spring Harbor perspectives in biology* 3.3 (2011): a001800.

Duband, J. L., et al. "Epithelium-mesenchyme transition during neural crest development." *Cells Tissues Organs* 154.1 (1995): 63-78.

Dude, Carolynn M., et al. "Activation of Pax3 target genes is necessary but not sufficient for neurogenesis in the ophthalmic trigeminal placode." *Developmental biology* 326.2 (2009): 314-326.

Dun, Xin-peng, et al. "Drebrin controls neuronal migration through the formation and alignment of the leading process." *Molecular and Cellular Neuroscience* 49.3 (2012): 341-350.

Ferguson, David P., Lawrence J. Dangott, and J. Timothy Lightfoot. "Lessons learned from vivo-morpholinos: How to avoid vivo-morpholino toxicity." *Biotechniques* 56.5 (2014): 251-256.

Fode, Carol, et al. "The bHLH protein NEUROGENIN 2 is a determination factor for epibranchial placode–derived sensory neurons." *Neuron* 20.3 (1998): 483-494.

Freter, Sabine, et al. "Cranial neural crest cells form corridors prefiguring sensory neuroblast migration." *Development* 140.17 (2013): 3595-3600.

Gagliardi, Delia, et al. "Stathmins and Motor Neuron Diseases: Pathophysiology and Therapeutic Targets." *Biomedicines* 10.3 (2022): 711.

Gaudillière, Brice, et al. "A CaMKII-NeuroD signaling pathway specifies dendritic morphogenesis." *Neuron* 41.2 (2004): 229-241.

Ge, Weihong, et al. "Coupling of cell migration with neurogenesis by proneural bHLH factors." *Proceedings of the National Academy of Sciences* 103.5 (2006): 1319-1324.

Geraldo, Sara, et al. "Targeting of the F-actin-binding protein drebrin by the microtubule plus-tip protein EB3 is required for neuritogenesis." *Nature cell biology* 10.10 (2008): 1181-1189.

Goodman, Corey S., and Nicholas C. Spitzer. "Embryonic development of identified neurones: differentiation from neuroblast to neurone." *Nature* 280.5719 (1979): 208-214.

Gordon-Weeks, Phillip R. "The role of the drebrin/EB3/Cdk5 pathway in dendritic spine plasticity, implications for Alzheimer's disease." *Brain research bulletin* 126 (2016): 293-299.

Grenningloh, Gabriele, et al. "Role of the microtubule destabilizing proteins SCG10 and stathmin in neuronal growth." *Journal of neurobiology* 58.1 (2004): 60-69.

Hallbook, F. I. N. N., et al. "Neurotrophins and their receptors in chicken neuronal development." *International Journal of Developmental Biology* 39.5 (2003): 855-868.

Hamburger, Viktor, and Howard L. Hamilton. "A series of normal stages in the development of the chick embryo." *Journal of morphology* 88.1 (1951): 49-92.

Hamburger, Viktor. "Experimental analysis of the dual origin of the trigeminal ganglion in the chick embryo." *Journal of Experimental Zoology* 148.2 (1961): 91-123.

Hardwick, Laura JA, and Anna Philpott. "Multi-site phosphorylation regulates NeuroD4 activity during primary neurogenesis: a conserved mechanism amongst proneural proteins." *Neural development* 10.1 (2015): 1-18.

Hayashi, Kensuke, et al. "Modulatory role of drebrin on the cytoskeleton within dendritic spines in the rat cerebral cortex." *Journal of Neuroscience* 16.22 (1996): 7161-7170.

He, Yan, Wenqian Yu, and Peter W. Baas. "Microtubule reconfiguration during axonal retraction induced by nitric oxide." *Journal of Neuroscience* 22.14 (2002): 5982-5991.

Heng, Julian Ik-Tsen, et al. "Neurogenin 2 controls cortical neuron migration through regulation of Rnd2." *Nature* 455.7209 (2008): 114-118.

Hou, Bing, et al. "Scalable and DiI-compatible optical clearance of the mammalian brain." *Frontiers in neuroanatomy* 9 (2015): 19.

Ji, Sheng-Jian, and Samie R. Jaffrey. "Intra-axonal translation of SMAD1/5/8 mediates retrograde regulation of trigeminal ganglia subtype specification." *Neuron* 74.1 (2012): 95-107.

Koontz, Alison, Hugo A. Urrutia, and Marianne E. Bronner. "Making a head: Neural crest and ectodermal placodes in cranial sensory development." *Seminars in Cell & Developmental Biology*. Academic Press, 2022.

Krus, Kelsey L., et al. "Loss of Stathmin-2, a hallmark of TDP-43-associated ALS, causes motor neuropathy." *bioRxiv* (2022).

Kuriyama, Sei, and Roberto Mayor. "Molecular analysis of neural crest migration." *Philosophical Transactions of the Royal Society B: Biological Sciences* 363.1495 (2008): 1349-1362.

Lassiter, Rhonda NT, et al. "Signaling mechanisms controlling cranial placode neurogenesis and delamination." *Developmental biology* 389.1 (2014): 39-49.

Lee, Jacqueline E., et al. "Conversion of Xenopus ectoderm into neurons by NeuroD, a basic helix-loop-helix protein." *Science* 268.5212 (1995): 836-844.

Lee, Vivian M., et al. "Both neural crest and placode contribute to the ciliary ganglion and oculomotor nerve." *Developmental biology* 263.2 (2003): 176-190.

Liebl, Daniel J., et al. "Absence of sensory neurons before target innervation in brain-derived neurotrophic factor-, neurotrophin 3-, and TrkC-deficient embryonic mice." *Journal of Neuroscience* 17.23 (1997): 9113-9121.

Ma, Qiufu, Chris Kintner, and David J. Anderson. "Identification of neurogenin, a vertebrate neuronal determination gene." *Cell* 87.1 (1996): 43-52.

Ma, Qiufu, et al. "neurogenin1 is essential for the determination of neuronal precursors for proximal cranial sensory ganglia." *Neuron* 20.3 (1998): 469-482.

Maharana, Santosh Kumar, and Jean-Pierre Saint-Jeannet. "Molecular mechanisms of hearing loss in Nager syndrome." *Developmental Biology* 476 (2021): 200-208.

McCabe, Kathryn L., John W. Sechrist, and Marianne Bronner-Fraser. "Birth of ophthalmic trigeminal neurons initiates early in the placodal ectoderm." *Journal of Comparative Neurology* 514.2 (2009): 161-173.

Mende, Michael, Nicolas AD Christophorou, and Andrea Streit. "Specific and effective gene knock-down in early chick embryos using morpholinos but not pRFPRNAi vectors." *Mechanisms of development* 125.11-12 (2008): 947-962.

Morii, Hiroshi, Yoko Shiraishi-Yamaguchi, and Nozomu Mori. "SCG10, a microtubule destabilizing factor, stimulates the neurite outgrowth by modulating microtubule dynamics in rat hippocampal primary cultured neurons." *Journal of neurobiology* 66.10 (2006): 1101-1114.

Moulton, Jon D., and Yi-Lin Yan. "Using Morpholinos to control gene expression." *Current protocols in molecular biology* 83.1 (2008): 26-8.

Moulton, Jon D. "Making a morpholino experiment work: controls, favoring specificity, improving efficacy, storage, and dose." *Morpholino oligomers* (2017): 17-29.

Nagashimada, Mayumi, et al. "Autonomic neurocristopathy-associated mutations in PHOX2B dysregulate Sox10 expression." *The Journal of clinical investigation* 122.9 (2012): 3145-3158.

Nan, Yuchen, and Yan-Jin Zhang. "Antisense phosphorodiamidate morpholino oligomers as novel antiviral compounds." *Frontiers in microbiology* 9 (2018): 750.

Parada, L. F., et al. "The Trk family of tyrosine kinases: receptors for NGF-related neurotrophins." *Cold Spring Harbor Symposia on Quantitative Biology*. Vol. 57. Cold Spring Harbor Laboratory Press, 1992.

Pataskar, Abhijeet, et al. "NeuroD1 reprograms chromatin and transcription factor landscapes to induce the neuronal program." *The EMBO journal* 35.1 (2016): 24-45.

Perez, Sharon E., Sandra Rebelo, and David J. Anderson. "Early specification of sensory neuron fate revealed by expression and function of neurogenins in the chick embryo." *Development* 126.8 (1999): 1715-1728.

Poobalasingam, Thanushiyan, et al. "The drebrin/EB3 pathway regulates cytoskeletal dynamics to drive neuritogenesis in embryonic cortical neurons." *Journal of Neurochemistry* 160.2 (2022): 185-202.

Powell, Lynn M., and Andrew P. Jarman. "Context dependence of proneural bHLH proteins." *Current opinion in genetics & development* 18.5 (2008): 411-417.

Schlosser, Gerhard. "Early embryonic specification of vertebrate cranial placodes." *Wiley Interdisciplinary Reviews: Developmental Biology* 3.5 (2014): 349-363.

Seo, Seongjin, et al. "Neurogenin and NeuroD direct transcriptional targets and their regulatory enhancers." *The EMBO journal* 26.24 (2007): 5093-5108.

Shah, Ankita, Andrew T. Schiffmacher, and Lisa A. Taneyhill. "Annexin A6 controls neuronal membrane dynamics throughout chick cranial sensory gangliogenesis." *Developmental biology* 425.1 (2017): 85-99.

Shan, Yufei, Stephen Matthew Farmer, and Susan Wray. "Drebrin regulates cytoskeleton dynamics in migrating neurons through interaction with CXCR4." *Proceedings of the National Academy of Sciences* 118.3 (2021): e2009493118.

Shiau, Celia E., et al. "Robo2-Slit1 dependent cell-cell interactions mediate assembly of the trigeminal ganglion." *Nature neuroscience* 11.3 (2008): 269-276.

Shiau, Celia E., and Marianne Bronner-Fraser. "N-cadherin acts in concert with Slit1-Robo2 signaling in regulating aggregation of placode-derived cranial sensory neurons." *Development* 136.24 (2009): 4155-4164.

Shiau, Celia E., Raman M. Das, and Kate G. Storey. "An effective assay for high cellular resolution time-lapse imaging of sensory placode formation and morphogenesis." *BMC neuroscience* 12.1 (2011): 1-11.

Shin, Jung Eun, et al. "SCG10 is a JNK target in the axonal degeneration pathway." *Proceedings of the National Academy of Sciences* 109.52 (2012): E3696-E3705.

Simões-Costa, Marcos, and Marianne E. Bronner. "Establishing neural crest identity: a gene regulatory recipe." *Development* 142.2 (2015): 242-257.

Singh, Sunita, and Andrew K. Groves. "The molecular basis of craniofacial placode development." *Wiley Interdisciplinary Reviews: Developmental Biology* 5.3 (2016): 363-376.

Singh, Aditi, et al. "Tcf12 and NeuroD1 cooperatively drive neuronal migration during cortical development." *Development* 149.3 (2022): dev200250.

Smith, Alexandra C., Stephen J. Fleenor, and Jo Begbie. "Changes in gene expression and cell shape characterise stages of epibranchial placode-derived neuron maturation in the chick." *Journal of anatomy* 227.1 (2015): 89-102.

Steventon, Ben, Roberto Mayor, and Andrea Streit. "Neural crest and placode interaction during the development of the cranial sensory system." *Developmental biology* 389.1 (2014): 28-38.

Theunissen, Frances, et al. "New perspectives on cytoskeletal dysregulation and mitochondrial mislocalization in amyotrophic lateral sclerosis." *Translational neurodegeneration* 10.1 (2021): 1-16.

Trainor, Paul A. "Craniofacial birth defects: The role of neural crest cells in the etiology and pathogenesis of Treacher Collins syndrome and the potential for prevention." *American journal of medical genetics Part A* 152.12 (2010): 2984-2994.

Urbán, Noelia, and François Guillemot. "Neurogenesis in the embryonic and adult brain: same regulators, different roles." *Frontiers in cellular neuroscience* 8 (2014): 396.

Xu, Hong, Carolynn M. Dude, and Clare VH Baker. "Fine-grained fate maps for the ophthalmic and maxillomandibular trigeminal placodes in the chick embryo." *Developmental biology* 317.1 (2008): 174-186.